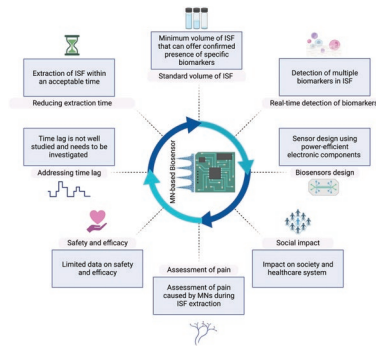


REVIEWS

K. M. Saifullah,
Z. Faraji Rad*2201763

Sampling Dermal Interstitial Fluid Using Microneedles: A Review of Recent Developments in Sampling Methods and Microneedle-Based Biosensors



Interstitial fluid is recognized as an important source of biomarkers; however, it is difficult and time-consuming to extract, thus limiting its use in medical diagnostic and clinical settings. Microneedles are minimally invasive devices that have gained extensive interest over recent decades. Microneedles can address some of the challenges associated with ISF extraction and sensing.

Sampling Dermal Interstitial Fluid Using Microneedles: A Review of Recent Developments in Sampling Methods and Microneedle-Based Biosensors

Khaled Mohammed Saifullah and Zahra Faraji Rad*

Although interstitial fluid (ISF) is recognized as an important source of biomarkers, it is difficult and time-consuming to extract, thus limiting its use in medical diagnostic and clinical settings. An inexpensive and effective technique for accessing ISF could benefit people with various health conditions and offer platforms for on-device sensing biomarkers. Microneedles (MNs) are minimally invasive devices that have gained extensive interest over recent decades. MNs can address some of the challenges associated with ISF extraction and sensing. Accessing ISF using MNs has the potential to develop advanced, non-invasive point-of-care (POC) microdevices that enable detection or continuous monitoring within the dermal ISF, therefore drastically impacting the healthcare system. This review describes recent studies exploring MN devices for ISF sampling and sensing. Several extraction processes, sampling volume, sampling duration, integration with biosensors, sensing of biomarkers, and subsequent analysis of ISF are discussed in detail. Furthermore, opportunities, conclusions, and future prospects for developing new research in the field are also discussed.

1. Introduction

Different body fluid sampling methods have been practiced for centuries, with many suffering from a phobia of needles and pain. In addition, pain associated with needle injections can cause anxiety and distress.^[1,2] Medical diagnosis often requires blood sampling and analysis of biomarkers. Early detection of these biomarkers has great potential to reduce the overall cost of both treatment and controlled monitoring of diseases.^[3,4] Traditional methods generally use a hypodermic needle to extract blood samples. This can cause infection^[5] and may not be available in remote locations or resource-limited settings, hindering

K. M. Saifullah, Z. Faraji Rad
School of Engineering
University of Southern Queensland
Springfield, Queensland 4300, Australia
E-mail: zahra.farajirad@usq.edu.au

 The ORCID identification number(s) for the author(s) of this article can be found under <https://doi.org/10.1002/admi.202201763>.

© 2023 The Authors. Advanced Materials Interfaces published by Wiley-VCH GmbH. This is an open access article under the terms of the Creative Commons Attribution License, which permits use, distribution and reproduction in any medium, provided the original work is properly cited.

DOI: 10.1002/admi.202201763

the provision of a patient-centric health-care system. Moreover, the risk associated with needle reuse, mainly found in developing countries, can cause severe health concerns for millions of people. Although most biochemical information about the body can be found in blood, other bodily fluids can also contain vital information. Due to the closed circulatory system, blood is maintained within blood vessel loops; thus, materials can only enter cells through the dermal interstitial fluid (ISF). ISF is mainly composed of water, surrounds various cells, and is a rich source of analytes such as electrolytes, proteins, amino acids, fatty acids, glucose, and other nutrients; and can provide critical data for disease diagnostics and continuous health monitoring.^[6–8]

Recent studies suggest that 83% of proteins found in the serum are also in ISF, but 50% of proteins found in ISF are not

in the serum. The results show high similarities in the diversity of proteins, where the differences were primarily reflected on a quantitative level.^[9] The proteomic analysis also indicates that the ISF proteome is fundamentally similar to plasma and serum proteome.^[10] Moreover, unlike serum and plasma, ISF will not clot, suggesting promising characteristics that it may be used as a substitute for blood or other biological samples for real-time diagnostics.^[6] Various methods have been studied to interpret the presence of biomarkers in ISF without any agreement on concentration.^[11,12] Many conventional methods of ISF sampling, such as suction blister, sonophoresis, reverse iontophoresis, microdialysis, and thermal ablation, can cause significant destabilization of the stratum corneum and local trauma.^[13] Additionally, other ISF extraction methods do not appear to be compatible with modern biosensor designs for detecting biomarkers and providing point-of-care (POC) service to help healthcare practitioners make immediate decisions for patient management.

In recent years, microneedles (MNs) have gained significant attention due to their micron size and minimal invasiveness. Pain associated with MNs insertion is significantly less than with a standard hypodermic needle.^[14] MN design parameters such as length, width, tip angle, or the number of needles can play a role in the pain level; in particular, MN length has the most effect on pain. Longer MNs (>1450 μm) may increase the pain score by several folds, whereas shorter MNs (<700 μm) are

significantly less painful during the insertion process.^[14] Fluid flow and pressure associated with infusion may cause pain during the MN insertion. However, different parameters, such as the amount of pressure, type of fluid, or insertion mechanisms, contribute to the pain level.^[15]

Integrating MNs with different biosensor technologies develops a robust and reliable system that can be accessed remotely to help healthcare practitioners make immediate decisions on patients' health. For this purpose, MN-based biosensors seem to be the approach that attains all the requirements of the POC system. Furthermore, these biosensors are described as minimally invasive to monitor biomarkers in ISF at a molecular level and typically coupled with MNs that extend no more than 1000 μm into the skin to extract ISF.^[14,16] To be adopted extensively into clinical practices, MN-based biosensors must also be capable of monitoring biomarkers over an extended period (e.g., days). In vivo evaluation can help to determine various performance factors (e.g., biocompatibility, selectivity, and reliability) of the biosensors in a biological system.

The traditional process of sampling ISF using MNs is challenging and relatively complex. Various research has been conducted primarily on MN-based drug delivery, leaving opportunities for further exploration and optimization of the ISF sampling process. **Figure 1** shows a comparison of publications in the areas of drug delivery and ISF extraction based on MNs. The data indicates a small number of research studies accomplished in ISF extraction compared to MN-based drug delivery systems. Furthermore, the standard required volume of ISF to confirm the guaranteed presence of biomarkers is yet to be explored and standardized.

It is believed that at some point in the future, most of the key biomarkers in ISF could be monitored by MN-based biosensors to provide critical insight into patients' health, enabling immediate medical action.^[18] One of the key challenges of POC diagnostics is integrating MNs into a compact system capable of real-time sampling of biofluids to provide an automated and accurate readout of patients' biomarkers. Microfluidic devices

can perform immunoassays with only a few nanoliters of biofluids. The concentration of sample constituents is an essential factor in providing information for diagnosing diseases.^[19–21] Analytical techniques are becoming ever more sophisticated and working with smaller concentrations of fluid, therefore paving the way for the development of lab-on-a-chip devices capable of sensing various biomarkers in the future.

Miniaturizing the size of hypodermic needles to a micron-size needle that is minimally invasive, less painful, easy to use, and has significantly less risk of infection, makes it one of the most prominent methods currently being developed for biofluid extraction. This review article describes the skin structure, physical characteristics, and pathways to access ISF. We review different ISF extraction techniques, primarily focusing on MN-based extraction and the use of MNs. Next, we critically discuss MNs integration with biosensors, in vivo analysis, and parameters for successful sensing and sampling of ISF. Finally, the challenges and existing barriers to sampling ISF and sample volume are explained. In addition, the implementation of the MN-based biosensors, critical research gaps, and future directions are discussed. Overall, this review seeks to deliver a realistic insight into the recent development of MN-based sampling and MN-based biosensors for sampling and sensing ISF. When designing MNs or MN-based biosensors, it is essential to recognize the current methods and their effectiveness in ISF sampling and sensing. By understanding the existing techniques and addressing their challenges, sampling time can be improved along with sampling volume. **Figure 2** illustrates an overview of different ISF extraction methods.

2. Skin Structure and ISF Sampling Pathways

Skin is the most accessible organ of the body and covers the body's entire external surface with a versatile structure.^[35] It contains three independent layers: the epidermis, dermis, and hypodermis (**Figure 3a**).

Publications in the area of Drug Delivery and ISF Extraction based on MNs

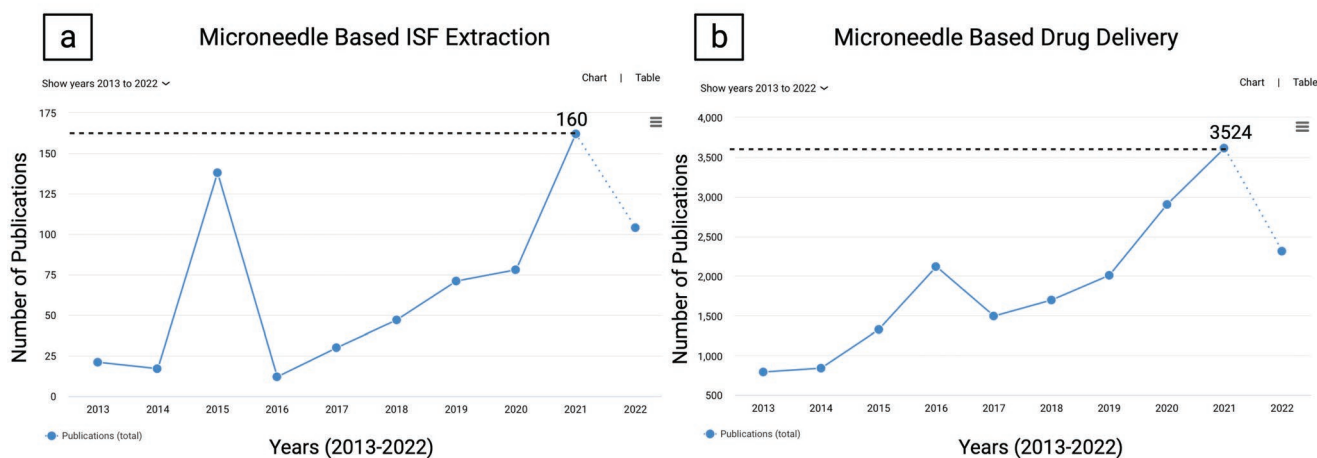


Figure 1. A comparison of an approximate number of research studies published between 2013–2022 in the area of a) MN-based ISF extraction and b) MN-based drug delivery.^[17] Accessed on 13th June 2022 under the license agreement.

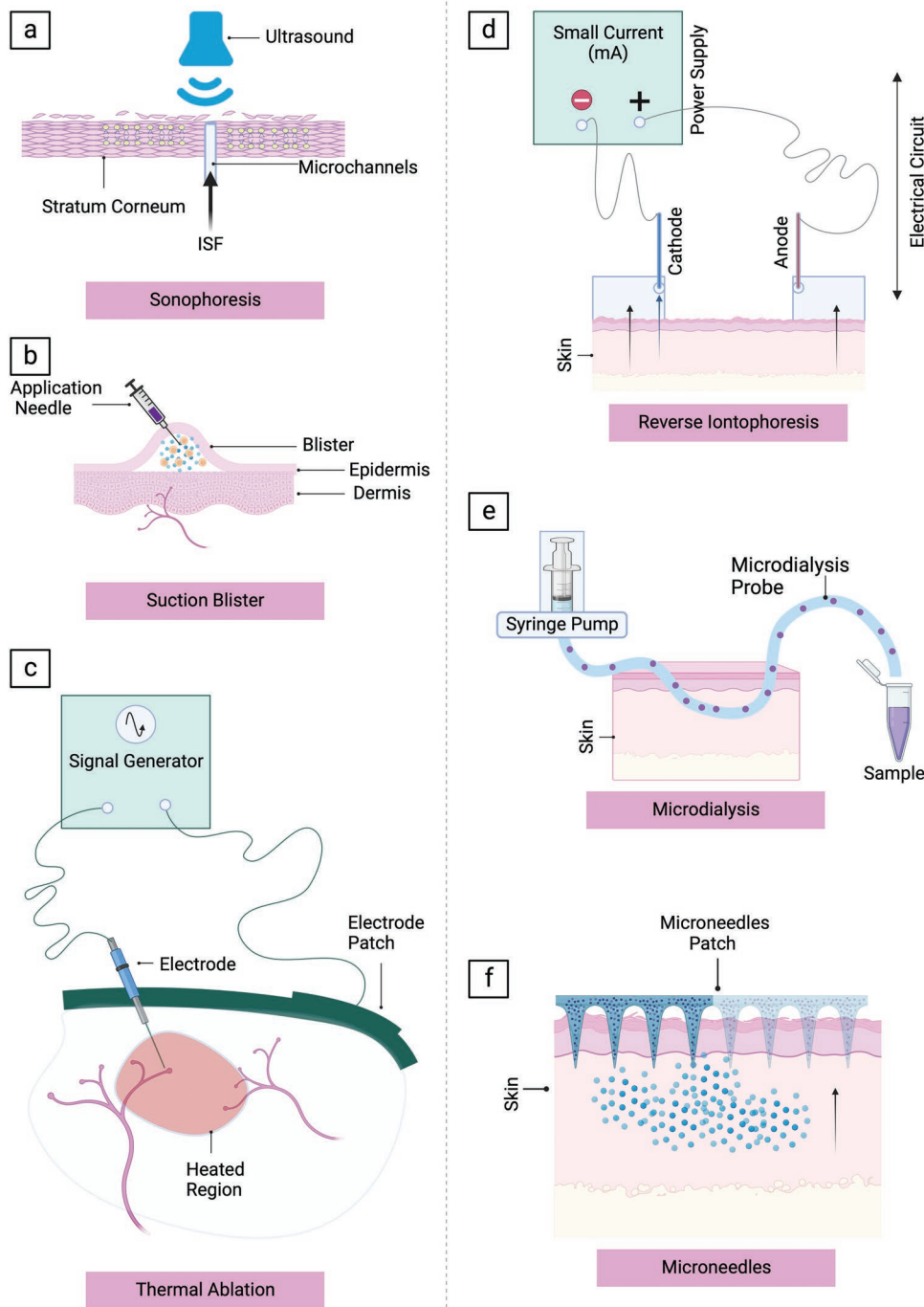


Figure 2. A schematic illustration of the different methods of ISF sampling. a) Sonophoresis—a low-frequency ultrasound applied to disrupt the stratum corneum.^[22] b) Reverse iontophoresis uses a small electric current and electrode to generate an electric field into the skin layer.^[23] c) Suction blister works by creating a blister using high temperature and using a needle for extraction.^[24–29] d) Thermal ablation works by skin ablation utilizing a high-voltage radiofrequency electrode.^[30] e) Microdialysis uses a dialysate pump and a catheter probe for substances to diffuse through the pore.^[31] f) MN patch to extract ISF.^[32–34] The schematic was created with BioRender.com.

A combination of these layers creates a distinct network to protect the body against UV lights, chemicals, and mechanical injuries.^[36] Epidermis, the uppermost layer, is extremely thin and does not have a direct blood supply.^[37] It is comprised of

five layers: stratum basale, stratum spinosum, stratum granulosum, stratum lucidum, and stratum corneum. These layers are mainly responsible for making new skin cells, giving skin its color, and protecting the body. The top layer of the epidermis,

Skin anatomy, ISF and Sampling Pathways

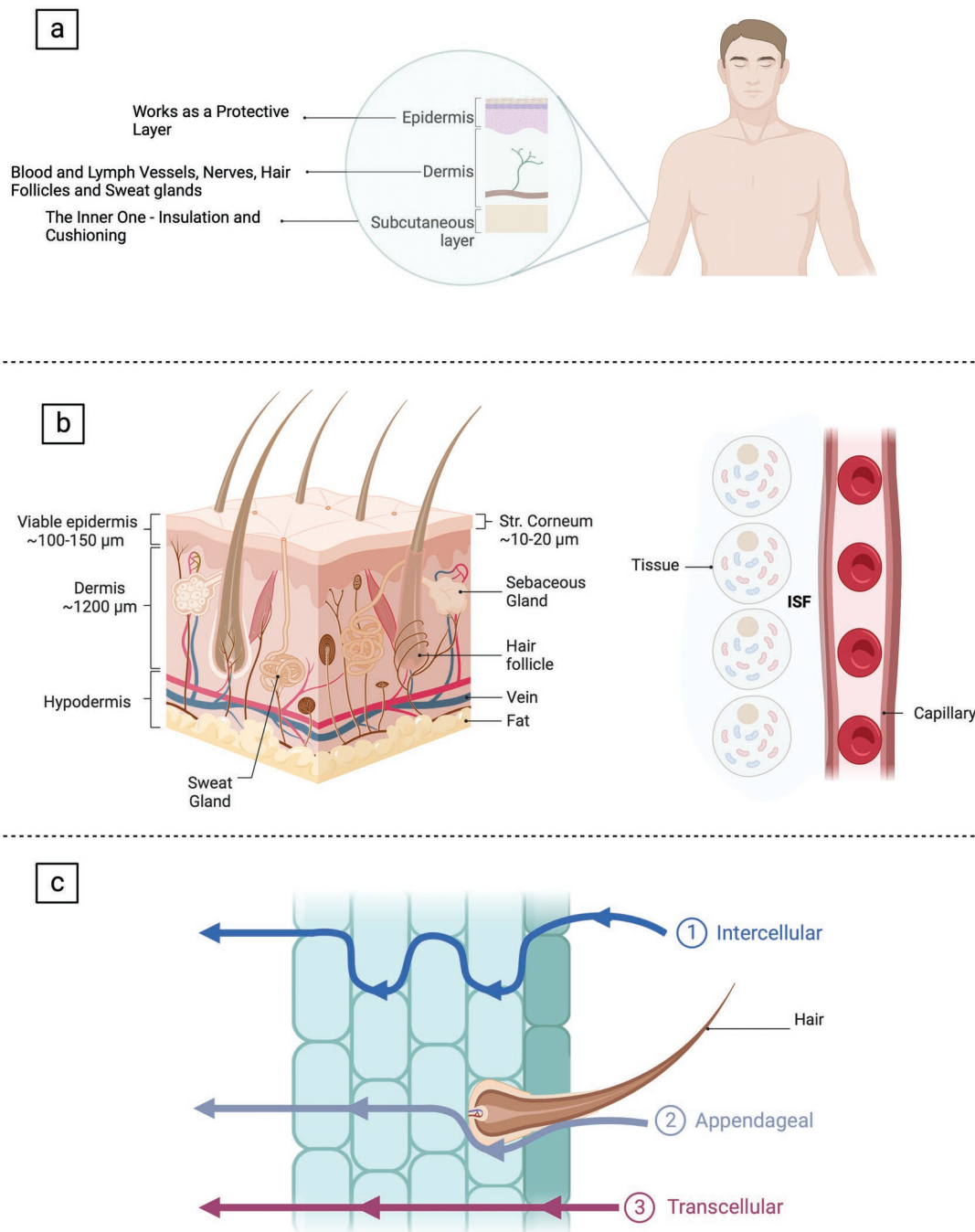


Figure 3. Illustration of the skin anatomy and ISF pathways accessibility in the skin. a) Characteristics of different layers and locations of the nerve system. b) Cross section of layers of the skin (left), and presence of ISF within the skin around tissue and capillary (right). c) Different pathways for ISF extractions. The schematic was created with BioRender.com.

the stratum corneum, is only 10–20 μm thick and most exposed to the outside environment.^[38] It is composed of several layers of keratin containing dead cells to prevent dehydration and retain water.^[36]

The dermis, the inner thicker portion, provides nutritional support to the epidermis layer. It is the thickest layer of the skin and is composed of elastic tissue providing flexibility to the skin. This layer contains nerve endings, blood supplies,

hair follicles, and sweat glands that support the skin's surface. The bottom layer, the hypodermis or subcutaneous layer, lies directly under the dermis and mainly includes fat and connective tissues. It works as a medium to store fat, provide insulation, and store energy (Figure 3b).^[36]

ISF can be accessed in three possible pathways (Figure 3c): intercellular, transcellular, and appendageal.^[39] The intercellular route is the passage through the intercellular space between cells to deeper skin layers. The in-between space consists of cholesterol, ceramides, and free fatty acids. One of the barriers to this route is the tight junctions in the intercellular space, which protect the skin from water loss. It has also been considered the primary penetration pathway for drug molecules.^[38] Suction blister and reverse iontophoresis are some of the methods used in this approach. Therefore, extraction techniques in this route are invasive and complex to accomplish in a small skin area. During the hydration gradient-driven transport, some nanoparticles can deform and penetrate through this route because the driving force behind such permeability is higher than the skin openings.^[40] The transcellular route collects ISF directly via the cells and is regarded as a shorter route than the intercellular path.^[41] This pathway is usually the predominant route for active transcellular transport and body fluid extraction. Therefore, depending on the corresponding technique, it can vary from minimally invasive to highly invasive. The use of hypodermic needles, MNs, and microdialysis techniques are some examples of this approach. The appendageal route offers rapid access to the deeper layer of the skin through sweat glands and hair follicles and can allow a unique passage for atypical penetrants.^[24] For example, the hair follicles on the skin may serve as the penetration site to deliver larger drug molecules or sense biomarkers in ISF. However, it is considered the most challenging path because the penetration of lipophilic and hydrophilic layers results in higher resistance in the passage.^[42,43] This route also has a high surface area and extended penetration depth ($\approx 2000 \mu\text{m}$) due to the presence of hair follicles.^[44,45] This route is receiving growing interest in diagnostics, mainly focusing on the use of nanoparticles.^[44] Nonetheless, no specific studies have been found to sample ISF through the appendageal route.

3. Current ISF Sampling Methods

ISF is an indicator source of biomarkers that can be used to diagnose and treat diseases. It can be sampled using various techniques such as suction blister, microdialysis, sonophoresis, reverse iontophoresis, thermal ablation, and MNs.^[13,25,27,28,30,31,24,46–49]

The following sections describe the conventional methods of ISF extraction and provide a detailed description of ISF sampling using MNs. **Figure 4** highlights the properties of different ISF sampling methods.

3.1. Sonophoresis

Low-frequency ultrasound increases the skin's permeability by disrupting the barrier property of the stratum corneum, the

outermost layer of the epidermis. The sonophoresis method uses vacuum pressure and low-frequency ultrasound to create micro-vibration in the epidermis.^[22] In clinical settings, this technique is mostly used for drug delivery. However, Pu et al. demonstrated an electromechanical sensor consisting of three electrodes integrated with a microfluidic chip to extract up to 1 μL of ISF.^[60] Ultrasound was used to improve the permeability of the skin, and the vacuum pressure enabled the successful extraction of ISF. A layer of graphene and gold nanoparticles (AuNPs) was used to improve the sensitivity of the electrochemical microfluidic sensor. Experimental results exhibited precise detection of glucose measurement and the potential to detect hypoglycemia minimally invasively.^[60] Although the combination of ultrasound and vacuum pump enhanced the extraction process, the extracted ISF scattered through the surface of the skin, similar to a dewdrop making it very difficult to collect. The longitudinal skin resistance of the ultrasonic area on the skin develops vertical micropores and good permeability, but it is also difficult to measure the longitudinal skin resistance precisely.^[61] Thus, the application of this technique has been very limited, and further studies are required for successful and repeated extraction of ISF. Generally, almost no pain is associated with this method, but the patient may experience slight heating of the skin during the process. Combined with other methods, such as integrating with MNs, it may reduce the extraction time of ISF sampling in diagnostic applications.^[51,52]

3.2. Reverse Ionophoresis

Ionophoresis applies a small electric current to the skin to increase the ISF flow. It involves the transportation of charged molecules through the passage of direct electric current. Under normal conditions, the subdermal ions move randomly and with almost constant concentrations. The epidermal layer comes under the influence of an electric field generated by an appropriate electrode. The charged molecules are attracted to their opposite poles promoting the transport of both charged and neutral molecules.^[23] Reverse iontophoresis uses an oppositely charged electrode to create the electric field. The current is applied via a power supply to the anode and cathode. Neutral and cationic ion molecules are dragged toward the cathode. Similarly, anionic components are drawn towards the anode chamber by electromigration, which enables the extraction of molecules into the skin's surface.

As voltage and current are the two most key parameters, application of higher current can cause erythema or redness. Thus, the appropriate current intensity with proper intervals is important, particularly in experiments with human volunteers.^[62]

Reverse iontophoresis has mostly received attention in glucose monitoring.^[63–65] Further applications may involve the detection and monitoring of other biomarkers. The primary factor that should be considered during this technique is maintaining the operating current density, as a strong current may damage the skin.^[53] This non-invasive technique also offers multiple sampling for patients subjected to frequent blood sampling procedures such as diabetes.^[54]

Properties of Different ISF Sampling Methods

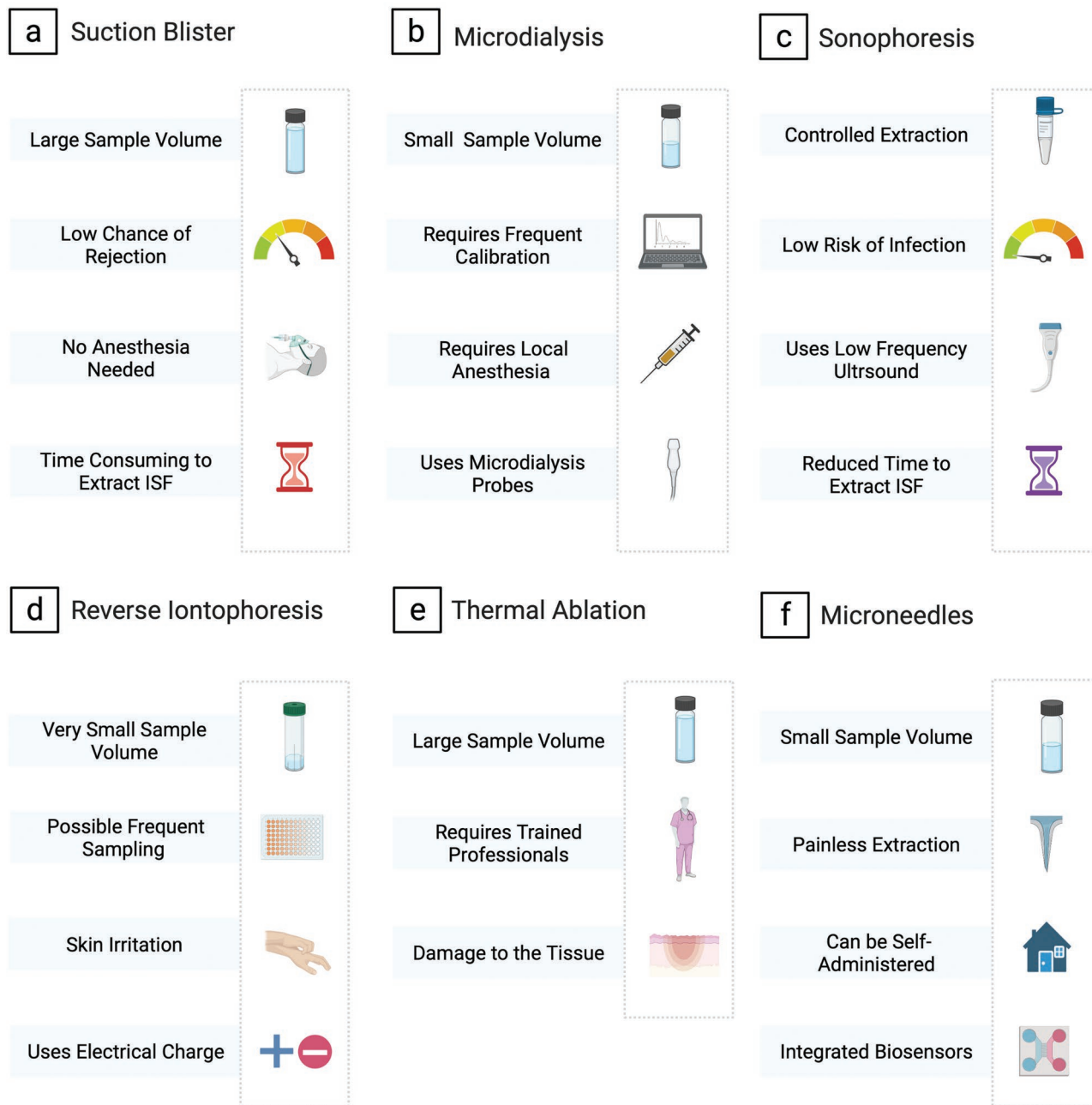


Figure 4. Schematic summarizes general properties of ISF sampling methods: a) suction blister,^[13,24–29] b) microdialysis,^[50] c) sonophoresis,^[51,52] d) reverse iontophoresis,^[47,53,54] e) thermal ablation,^[55,56] f) microneedles (MNs).^[57–59] The schematic was created with BioRender.com.

3.3. Suction Blisters

The suction blisters method is commonly used to extract or sample a higher volume of ISF by applying negative pressure to the skin at a high temperature for several minutes up to an hour.^[24–29] The dermis and epidermis are separated when an external suction application is applied. The suction generates

a gap that is filled by the fluid from surrounding cells, creating blisters filled with ISF. This occurs within the epidermis area, and the fluid is usually colorless (known as suction blister fluid [SBF]). A needle or syringe is then used to extract the sample, mainly consisting of ISF. **Table 1** shows some of the properties and parameters of suction blister methods used to extract ISF by researchers. The challenges involved in this method are

Table 1. Properties of the suction blister methods used to extract ISF.

Pressure	Object	Temperature	Duration	ISF volume	Year [Ref.]
40–55 kPa	Forearm	–	1.30 h	50–200 μL	2020 ^[66]
50–70 kPa	Thigh	40 °C	\approx 45 min	50 μL	2018 ^[67]
20–30 kPa	Forearm	–	12–24 h	\approx 500 μL	2018 ^[68]
25–40 kPa	Forearm	–	>2 h	30–100 μL	2007 ^[6]

1) side effects such as injury at the site of treatment, 2) infection, and 3) skin discoloration, all of which usually require a prolonged time to heal.^[13]

3.4. Thermal Ablation

Similar to sonophoresis, the radiofrequency thermal ablation method can be used to create micropores. Applying a high-voltage radio frequency electrode on the skin triggers ions within the cells to follow the direction change of the applied current. This generates heating of the tissue and creates an ablation of the stratum corneum in the application area. A comparatively higher volume of ISF (\approx 0.5 $\mu\text{L min}^{-1}$) can be extracted by this method, where the number of micropores is generally proportional to the ISF volume.^[30] However, thermal ablation can cause redness, infection, and injury to the tissue.^[55]

3.5. Microdialysis

The microdialysis technique has been used for sampling ISF and delivering drugs. This method involves exchanging substances within a semipermeable membrane and is primarily based on diffusion.^[31] A simple microdialysis system uses a dialysate pump and a catheter or probe made of a semipermeable dialysis membrane that enters the tissue's fluid. The pump creates a flow for the fluid towards the probe or catheter. For diffusion exchange to occur, perfusion fluid is flown at a slow rate (0.5–5 $\mu\text{L min}^{-1}$) across the semipermeable membrane of the probe.^[46] Substances (e.g., glucose) diffuse through the membrane's pores and can be collected for further analysis. This technique is mainly used to continuously monitor analytes, such as glucose, and gather information about local drug concentrations in the skin.^[69–71] Microdialysis requires the insertion of the probe directly into the skin to sample ISF, and can cause discomfort during the test. The application of the technique for ISF sampling requires local anesthesia-trained professionals and a longer time to obtain a small sample volume. The probe also needs calibration, and the patient can experience tissue trauma.^[50]

3.6. MNs for ISF Sampling

To extract ISF effectively, the methods explained above require a long sampling time, calibrations, specialized equipment, and trained professionals. Applications of these methods are mostly limited, except for measuring glucose concentration.^[57] Additionally, a typical hypodermic needle is usually long (>16 mm)^[72]

and pierces the skin at a low angle to reach deep into the capillary to extract blood.^[73] The process is semi-invasive, requires trained healthcare professionals, and produces biohazard waste.^[74] An alternative approach for collecting ISF is using MNs for simple and effective extraction of ISF. MNs are usually not long enough to reach the pain receptors and will bypass the stratum corneum barrier by creating micrometer pathways for ISF transport. In addition, MNs cause lower microbial penetration than hypodermic needles.^[75] MNs generally range from 25–2000 μm in height and can be made of different materials and shapes using various micro and nanofabrication techniques.^[76] The four major types of MN design are solid, hollow, dissolving, and hydrogel, and they were initially developed for drug delivery.^[32–34] MNs have also successfully extracted micron and nanoliter volumes of ISF and have shown promising results for biomarker collection for disease diagnosis. Various design considerations have also been explored such as overall geometry, length, diameter size, array density, and materials.^[77] The following sections describe how researchers have used each MN to sample the skin's ISF. **Figure 5** illustrates different types of extraction principles for each MN type.

3.6.1. Solid MNs for Direct ISF Sampling

Solid MNs are robust structures designed to penetrate the stratum corneum of the skin, which can be made of materials such as silicon, metals, and polymers.^[57] Solid MNs cannot extract ISF directly but can be integrated with other techniques for the minimally invasive extraction of ISF. These types of MNs are simpler to manufacture, mechanically robust, and more cost-effective to manufacture than other designs. The process primarily contains two stages: 1) successful insertion of MNs into the skin and 2) accumulation of ISF by various methods, such as coupling the MN device with a paper reservoir to absorb the extracted ISF from the skin or techniques such as suction, pressure-driven convection, diffusion, and osmosis.^[58] Kolluru et al. reported a cost-effective method for sampling ISF using solid MN patches and paper reservoirs (**Figure 6a**). The study used 650 μm long MNs fabricated from stainless steel using an infrared laser. The patch was developed as a two-part system comprised of five to nine MNs inserted into the skin multiple times at an angle of 10–45° enabling the flow of ISF out of the skin and into the paper. The paper acted as a reservoir for the ISF collection.^[57] When using a paper reservoir, the paper's absorptiveness and percentage of porosity may impact the time required to sample ISF. As a result, different strip papers were experimented with, and the filter paper was chosen as the reservoir material due to its availability and widespread use in designing paper-based devices.^[78,79] The

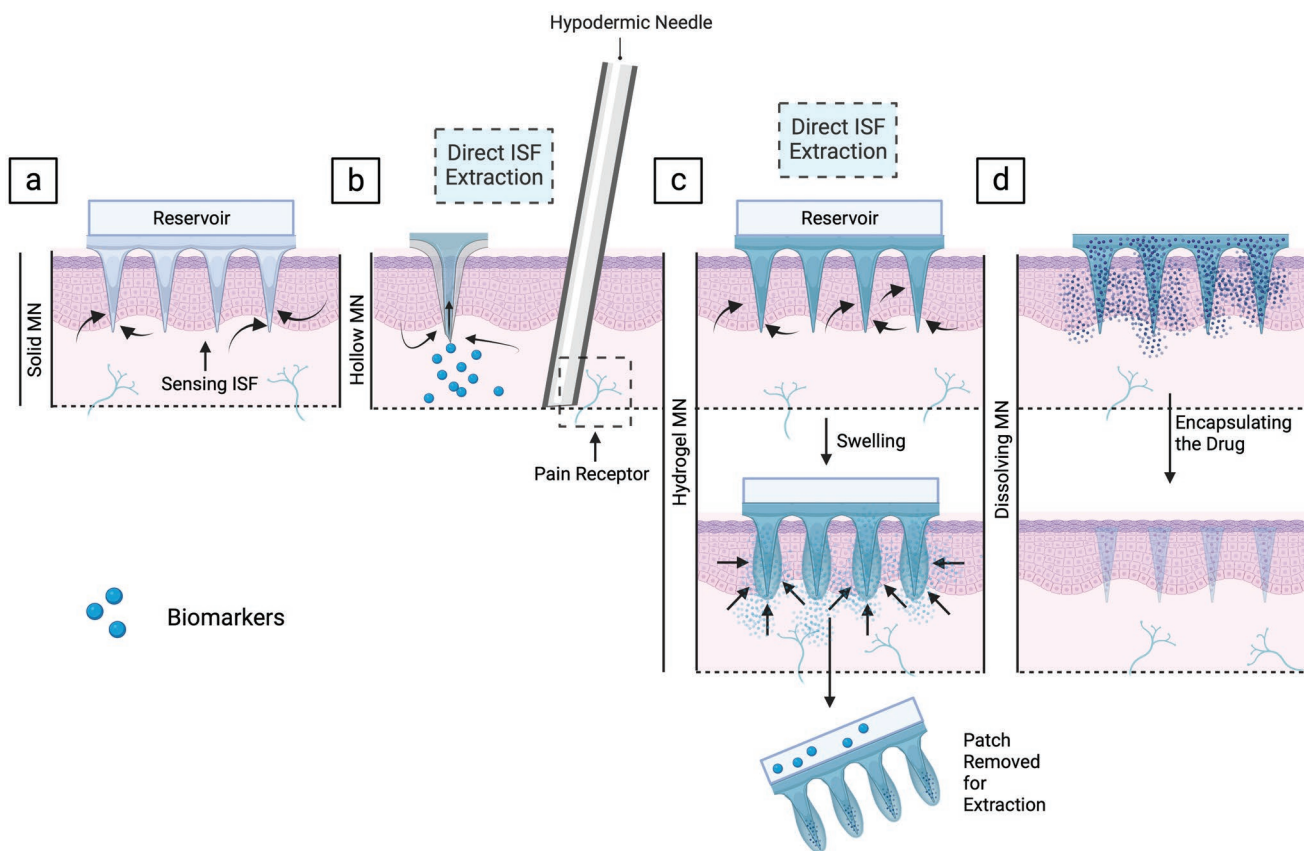


Figure 5. Illustrative comparison between different types of MNs and a hypodermic needle. a) Solid MNs must be integrated with other techniques for extracting and sensing ISF. b) Hollow MNs for direct extraction of ISF. c) Illustrated diagram of hydrogel MNs patch for extracting ISF. Hydrogel MNs inserted into the skin, the swelling process drives the ISF to diffuse into the patch. Then, the patch is removed for further analysis. d) Dissolving MNs patch, mainly for drug delivery. The schematic was created with BioRender.com.

experiment was conducted on fifteen female Wistar rats *in vivo* and pig cadaver skin *ex vivo*. The results showed that, within a minute, $>2 \mu\text{L}$ of ISF was extracted from the rat skin *in vivo*. The results also demonstrated that air plasma treatment of MN arrays in a plasma chamber for 5 min increased the capability of the MN patches to extract ISF. However, the study did not address any pain associated with ISF collection, and the side effects of multiple insertions of solid MNs into the skin were not discussed.^[57]

Another mechanism is to apply solid MNs for ISF extraction from the skin using pressure difference to transport ISF from the skin into the micropores created by MNs or to a reservoir. Fluid flow out of the skin occurs due to the pressure difference between the fluid and the external pressure. Generally, arrays with high needle density have shown improved flow rates.^[80] Additionally, the effects of pressure gradients have been studied and optimized to achieve higher flow rates in sampling ISF using MN patches. For instance, Samant et al. used a MN patch with enhanced pressure gradients to extract up to $10 \mu\text{L}$ of ISF within 2 min. The MNs patch was made of stainless steel with two separate steel plates joined together on top of each other, and an absorbent paper was sandwiched between the plate layers using adhesive. For sampling, the experiment was conducted on pig skin *ex vivo* and rat skin *in vivo*. Initially, the patch was inserted for two minutes, and an external transverse

force ($\approx 44.4 \text{ N}$) was applied to the site. Results demonstrated successful penetration of the MNs to extract clinically relevant volumes of ISF. The volume of the ISF absorbed by the paper was found to be dependent on the force applied.^[48]

A challenge during the extraction of ISF is to ensure there is no contamination with capillary blood due to the high vascularity of the skin. ISF is colorless due to a lack of red blood cells and can be confirmed by microscopic analysis. Applying a vacuum to the micropores created on the skin by MNs can contaminate ISF with blood. Although blood vessels and capillaries are deeper into the dermis, designing an optimized MN array and using an optimum vacuum pressure during insertion and collection reduces the risk of bleeding. For example, in one study MN patches were coupled with mild suction to sample clinically relevant amounts of ISF from human participants. The MN patch was applied to create the micropores on the skin, and vacuum pressure as low as -50 kPa (gauge) was used for 20 min to extract the ISF. Then, MNs of 250, 450, and $650 \mu\text{m}$ in length were inserted into the skin, followed by the application of a vacuum at -34 , -50 , and -17 kPa (gauge). All tests resulted in bleeding, especially at $650 \mu\text{m}$ length. The results indicate that inserting MNs with $250 \mu\text{m}$ in length can reduce the chance of bleeding by 60%. The vacuum chamber was aligned with the skin and had a bottom plate with up to five orifices connecting the vacuum to the skin. After applying

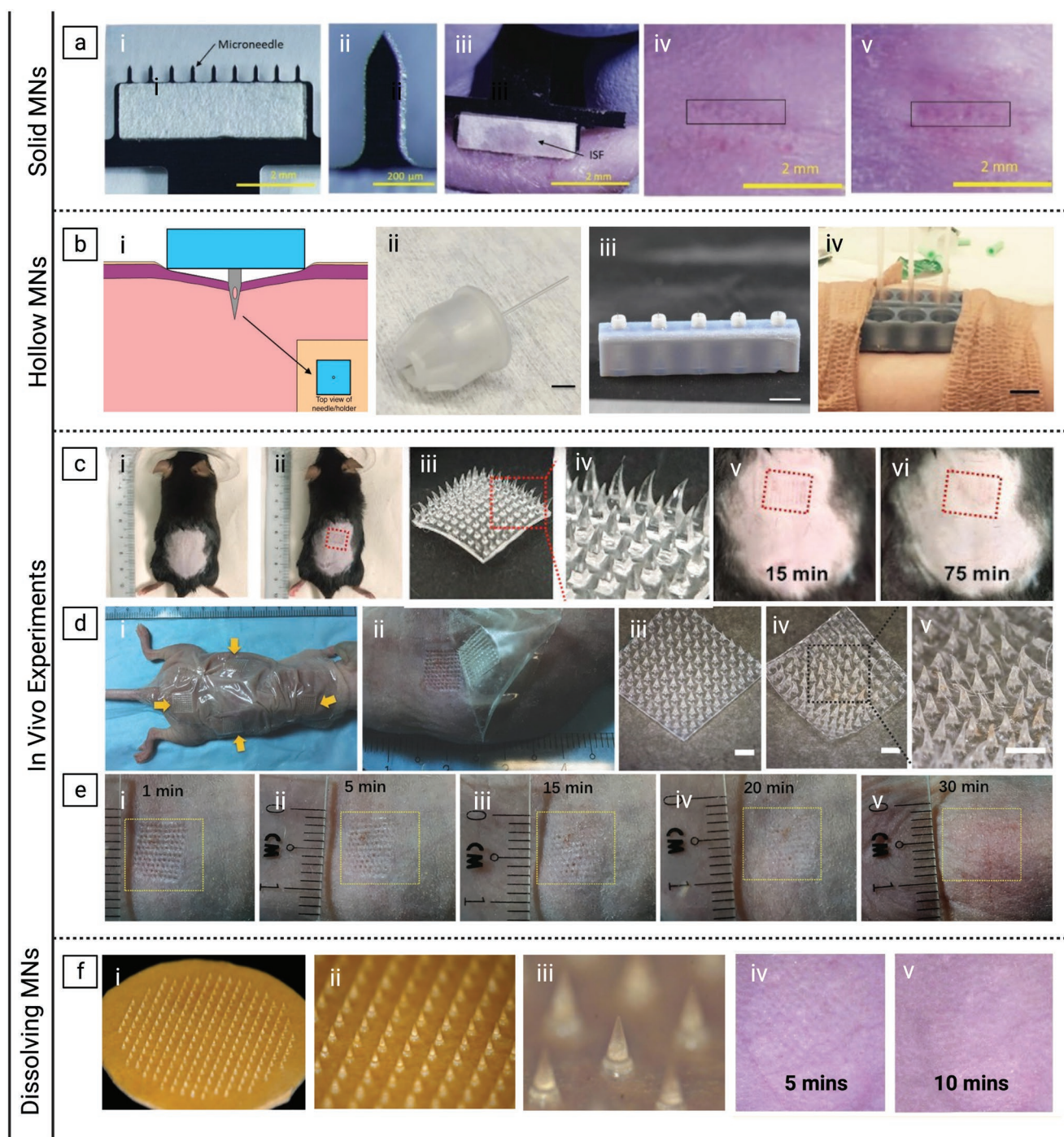


Figure 6. Application of MN array in extraction of ISF. a) i) MN patch showing a row of nine MNs, ii) Magnified image of the MN, iii) MN patch penetrating the skin of a hairless rat *in vivo*, iv) skin after 10 times insertion of the MN patch, v) 5 min after 10 times insertion of the patch. Reproduced with permission.^[57] Copyright 2019, Wiley-VCH. b) i) MN configuration, inset showing the top view, ii) single MN with a capillary collection tube, iii) customized 3D printed MN holder, iv) two MN holders joined for the extraction of ISF in glass capillary tube. Reproduced under the Creative Commons Attribution License (CC BY 4.0).^[91] Copyright 2018, Springer Nature. c) i) Image of the shaved mouse back before the insertion of the MN patch, ii) After the insertion, iii) Mal2–MeHA MN patch after insertion, iv) Magnified image of the MNs tip after the insertion, v) skin recovery after 15 min, (vi) 75 min after the experiment. Reproduced with permission.^[101] Copyright 2020, Wiley-VCH. d) i) MN patch inserted into the skin of the mouse back and attached by Tegaderm film, ii) Visible micro holes appeared on the skin after penetration, iii–v) Magnified images of the MN patch after removal from the skin. Reproduced with permission.^[99] Copyright 2017, Wiley-VCH. e) Visualization of the MN insertion site and skin recovery within 30 min post-experiment. Reproduced with permission.^[99] Copyright 2017, Wiley-VCH. f) i) An array containing 225 dissolving MNs, ii) a close-up view of the array, iii) enhanced image of the MNs, iv) 5 min, v) 10 min after the insertion into the tissue. Reproduced under the Creative Commons Attribution License (CC BY 4.0).^[100] Copyright 2016, Ivyspring International.

the vacuum at -50 kPa for 20 min and slowly reducing it over three minutes, the vacuum was stopped, and the orifice plate was removed. ISF was visible on the skin and collected using sterile medical gauze. This technique prevented ISF to be evaporated during the extraction process. This optimized process resulted in the collection of 2.3 ± 2.6 μL of ISF within 20 min without any visible traces of blood. The results also showed that ISF collection was varied among individual micropores across a MN patch even though all participants received the same treatment, with the majority of the micropores not contributing to the collection of ISF.^[81]

Another study used a two-stage approach using solid MNs and a mild vacuum for ISF extraction. The MN arrays were tested on the skin of anesthetized hairless rats and human subjects. A vacuum of 200–500 mm Hg for 2–10 min was applied to extract ISF to analyze glucose concentration, and 1–10 μL of ISF was extracted within 2–10 mins. However, the vacuum extraction caused local erythema in the human subjects, which persisted for a few hours.^[82]

Solid MNs have shown promising results in collecting ISF from the skin. However, due to their solid nature, this type of MN must be integrated with other mechanisms (such as a vacuum) for administration. This can complicate ISF sampling and the development of miniaturized POC devices.

3.6.2. Hollow MNs for Direct ISF Sampling

Hollow MN designs contain an internal channel that relies on capillary force to draw ISF from the skin. Hollow MNs have been fabricated in different heights and geometries, mainly from metals, silicon, glass, ceramic, and polymers^[49] using dry etching,^[83] 3D printing,^[84] two-photon polymerization,^[85–87] and drawing lithography^[88] techniques. ISF extracted by capillary flow increases the concentration gradient in the neighboring dermis area. As a result, the sampling process is comparatively faster than hydrogel MNs or micropore systems created by solid MNs.^[58] However, one primary concern of hollow MNs is the blockage of channels due to entrapped dermal tissue.^[89,90]

Unlike other sampling methods such as microdialysis or suction blister, hollow MNs can extract ISF without expensive or complicated arrangements. For example, Miller et al. experimented with three different MNs lengths (1000, 1500, and 2000 μm) to test the ability of each MN to extract ISF without the need for any separate instrument such as a vacuum. The MNs were made from stainless steel with a glass capillary attached to the backing of the MNs and were applied to human subjects (Figure 6b). Although ISF was extracted with all three MN lengths, the MN with 1500 μm height exhibited a higher extraction percentage than others. The results showed up to 16 μL of ISF was extracted within 2 h,^[91] improving overall efficiency compared to other similar studies which reported an average of 1 μL of the sample being collected in 30 min.^[82,92] The MNs were pre-lubricated, and the design was modified to reduce insertion penetration force. The array was fabricated using a 3D printer containing five MNs upholding concentric design.^[91] Taylor et al. further investigated the effect of the MN holders in ISF extraction by varying the design parameters (e.g., holder throat thickness and tip curvature). Initially, four MNs

were designed (flat, concave, convex, and beveled) and 3D printed with four MN arrays. Each consists of MNs with an insertion depth of 1000 and 1500 μm . Results reported that ISF extraction could be affected by the different design parameters of the MN holder. Concave tip design had significantly improved ISF extraction rate and was suggested as optimal for ISF extraction in animals.^[93] Samant et al. reported inserting a hollow MN with a single capillary system which extracted >1 μL of ISF within 20 min. The fabricated MN was 750 μm in length, made of stainless steel, and applied to the pig cadaver skin for 20 min to collect ISF. The method used in this study was very slow, and a low volume of ISF was collected, which can be an issue for further analysis of the sample.^[58] Pain associated with hollow MN insertion has been assessed by visual-analogue scale score and reported to be less than a hypodermic needle. For example, Gupta et al. reported a 1000 μm length hollow MN to deliver insulin effectively in two subjects with type-1 diabetes. The subjects did not report any pain during the insertion.^[94] In another study, Norman et al. developed a hollow MN array inserted into patients' abdomens for insulin delivery. The pain for the insertion was assessed by visual-analogue scale score, and MNs were found to be less painful than a hypodermic needle.^[95,96] However, hollow MNs are comparatively weaker and may suffer leakage and clogging during insertion.^[97,98] **Table 2** summarizes recent ISF extraction studies using different MN materials emphasizing the ISF extraction volume.

3.6.3. Hydrogel MNs for Direct ISF Sampling

The hydrogel MN is a relatively new type of MN and was first introduced in 2010.^[107] Diffusion is another mechanism for ISF sampling that can be established using dry hydrogel MNs. When inserted into the skin, the swelling characteristics of the hydrogel MN causes the material to swell and rapidly take up ISF from the tissue, making them suitable for self-administration in biomedical applications. The collected ISF can be used as a biomarker source for disease diagnosis. Hydrogel MNs are mainly made of polymers, are relatively easy to fabricate, and have high mechanical strength in dry conditions.^[108] PVA (polyvinyl alcohol) is a widely used and researched polymer for developing hydrogel MNs due to its nontoxicity and biocompatibility.^[109] The use of several PVA/polymer combinations, such as carboxymethyl cellulose (CMC)^[110] and chitosan (CS)^[110] have been reported. It enhances the specific properties of the MNs by incorporating them with other polymers. Although it is reported to have a slow swelling rate,^[111] the biocompatibility of the PVA makes it more effective compared with other methods. For example, Samant et al. reported using crosslinked PVA-based hydrogel MNs to extract ISF. A patch of 100 MNs was applied to the skin for 12 h. The results showed that each MN could extract 0.0030 μL of ISF from the skin, and the effectiveness of these hydrogel MNs was greater than hollow MNs.^[58]

However, the process takes longer due to the properties of the hydrogel MNs absorbing high levels of water inside the physical structure of the material. To address the issue, He et al. fabricated a hydrogel MNs patch made of PVA and chitosan (CS) containing 100 MNs for monitoring glucose. The combination of PVA and CS gave the structure enough

Table 2. Summary table of the ISF extraction using different MNs discussed in this review.

MNs	Materials	Length	Object model	Duration	ISF volume	Year [Ref]
Solid MNs	Stainless steel	250–650 μm , 5 MNs	Human participant	Within 20 min	$2.3 \pm 2.6 \mu\text{L}$ (optimized)	2020 ^[81]
	Glass	$\approx 700\text{--}1500 \mu\text{m}$	Anesthetized hairless rats	2–10 min	1–10 μL	2005 ^[82]
	Stainless steel	1000 μm , 5 MNs, 2 layers	In vivo hairless rat ex vivo pig skin	Within 2 min	–	2015 ^[48]
	Stainless steel	650 μm , 9 MNs 750 μm , 5 MNs	In vivo hairless rat ex vivo pig skin	Within 1 min	$>2 \mu\text{L}$	2019 ^[57]
Hollow MNs	Stainless steel	1000 μm , 1500 μm , 2000 μm 5 MNs	Human participant Rat skin	Within 1–2 h	Up to 16 μL	2018 ^[91]
	Stainless steel	250 μm	Human participant	Within 20 min	$\approx 0.01\text{--}0.03 \mu\text{L}$	2018 ^[58]
Swellable MNs	Methacrylated hyaluronic acid (MeHA)	800 μm , 100 MNs	Mice skin	≈ 1 min ≈ 10 min	$1.4 \pm 0.3 \mu\text{L}$ $2.3 \pm 0.4 \mu\text{L}$	2017 ^[99]
	Chondroitin sulfate	$501.8 \pm 2.1 \mu\text{m}$, 225 MNs	Male Wistar rats	≈ 15 min	2 μL	2016 ^[100]
Hydrogel MNs	Osmolytes and hydrogel	900 μm	Ex vivo pig skin in vivo mouse skin	Within 3 min	7.90 μL (pig) 3.82 μL (mouse)	2020 ^[101]
	Polyvinyl alcohol (PVA) and Chitosan (CS)	$1266 \pm 91 \mu\text{m}$, 100 MNs	In vivo rabbit skin	≈ 10 min	$1.25 \pm 0.37 \mu\text{L}$	2020 ^[102]
	–	550 μm , 7 \times 7 arrays	Human skin	Within 2 min	6.5 μL	2019 ^[103]
	Polyvinyl alcohol (PVA) /poly- vinylpyrrolidone (PVP)	600 μm –1000 μm 10 \times 10, multiple patches	Rat skin	Within 12 minutes	4.4 μL	2022 ^[104]
	Gelatin methacryloyl (GelMA) and graphene oxide (GO)	600 μm 100 MNs, 10 \times 10 array	Mouse skin	Within 30 min	21.34 μL	2022 ^[105]
Sponge Forming MN	Polyvinyl formal (PVF)	680 μm , 12 \times 12 array	Rat skin	Within 1 min	1.6 μL	2019 ^[106]

stiffness to penetrate the tissue without breaking and offered a high porosity and swelling ability to collect ISF. In this study, the MN patch was inserted into the rabbits' skin to extract ISF; $1.25 \pm 0.37 \mu\text{L}$ of the sample was withdrawn within 10 min. The extraction process continued for 24 h to understand the possibility of frequent use of the patch. To investigate the viability of the system, the results of MN patches were compared against the standard rabbit blood test using the commercial glucometer, indicating a correlation between the data obtained from both methods.^[102]

PVA has also been used with PVP (polyvinylpyrrolidone) to improve the overall swelling properties of MN patches, thus making the MN patch more effective in ISF extraction within a short time and without the need for any additional device. One study suggests that a PVA MN patch could only extract 0.3 μL of ISF.^[58] A combination of PVA and PVP in MN patch formation produced a higher extraction volume of ISF. For example, Xu et al. used a combination of PVA/PVP for the MNs patch with improved swelling properties and extracted 4.4 μL of ISF within 12 min. The effectiveness of extraction was also assessed using different ratios of PVA/PVP. The results showed PVA/PVP MN patches with a 2:1 ratio exhibited strong extraction ability.^[104]

Hydrogel MNs consisting of gelatin methacryloyl (GelMA) and graphene oxide (GO) have also been used for ISF extraction and biomarker detection. GelMA has excellent biocompatibility and has been constructed in various scaffolds, showing robust sampling properties during biomedical applications.^[112] Furthermore, the low viscosity characteristics of GelMA offer

minimal invasiveness and sensitive detection. A study by Qiao et al. fabricated a MN patch using GelMA and GO to extract ISF and detect multiple microRNAs (miRNA). The patch containing 100 hydrogel MNs was applied to the back of the psoriasis mouse model and sampled 21.34 μL ISF in 30 min. The introduction of GO and GelMA into the MNs improved the effectiveness of the extraction process, making monitoring disease progression more feasible.^[105]

Alternative materials such as methacrylated hyaluronic acid (MeHA) have also been explored to increase the swelling rate and extract a sufficient volume of ISF.^[113] Hyaluronic acid (HA) is available naturally in the body and shows excellent biocompatibility. Its water-soluble characteristics cause it to break down into the skin, but this can be resolved by synthesizing HA with MeHA.^[114] Zheng et al. reported an osmosis-powered hydrogel patch with 100 MNs fabricated with MeHA and osmolyte (maltose) that can extract ISF three times faster than normal hydrogel MNs (Figure 6c). The study suggested that the higher swelling ability of the fabricated MN device can increase the amount of ISF in a shorter period. During the process, dissolving osmolytes provided the osmotic pressure to drive the diffusion of ISF into the hydrogel matrix. The results showed the patch could sample 7.90 μL of ISF from pig skin ex vivo and 3.82 μL of ISF from mouse skin within 3 min compared to the same patch that took 10 minutes without the osmolyte.^[101] In another study, Sulaiman et al. developed a MN patch coated with hybrid alginate-PNA hydrogels and extracted $\approx 6.5 \mu\text{L}$ within 2 min. The MNs were designed in a pyramidal shape with a height of 550 μm for each needle,

enabling them to penetrate the skin epidermis layer to access ISF. The model achieved 63% of full swelling capacity within a minute, showing positive results compared to other hydrogel-coated MN sampling techniques.^[103] Superabsorbent acrylate-based hydrogels have also been used in the development of MN patches. These hydrogels are capable of absorbing water at a significantly higher volume.^[115] Laszlo et al. utilized this advantage to develop MN patch that successfully extracted 6 μL of ISF within 15 min. Initially, two types of MN patches were designed for dermal ISF proteomics sampling. The in vitro and in vivo biocompatibility tests were conducted for proteomic analysis. The developed MN patch could withstand and recover the initial shape even after the washing steps. The results demonstrated that MN chemistry (e.g., crosslinking, synthesizing) has a significant influence on ISF extraction, as specific biomarkers could be detected by modifying the composition of the MN patch.^[116] Chang et al. also described a swellable MN patch that can extract $2.3 \pm 0.4 \mu\text{L}$ of ISF in 10 min (Figure 6d,e). The MN patch was composed of MeHA, which was UV crosslinked. Because of MeHA's high water uptake, this MN patch could extract enough ISF quickly without using additional devices, improving the overall metabolic analysis. The MN patch retained structural integrity leaving no residue on the skin after use.^[99]

3.6.4. Dissolving MNs

Dissolving MNs are biocompatible, more dose effective, and generally do not generate biohazard waste.^[117,118] They are made of water-soluble materials such as biocompatible polymers, sugars, sodium, chondroitin, sulfate, or hyaluronic acid and can be self-administered in drug delivery. During insertion, the tip of the MNs dissolves, and dissolution takes place to release the drug. Although patches are used to facilitate the process, the efficacy of drug delivery is often reduced because of the variation in skin elasticity which can lead to the dissolving MNs being inserted incorrectly.^[119–121] Controlled drug delivery can be achieved by modifying polymer composition.^[122] Dissolving MNs have also been demonstrated to be more dose-effective than subcutaneous dose delivery.^[117,118,123] Despite being used primarily in drug delivery, Ito et al. showed the potential use of dissolving MNs in ISF extraction. They developed a patch containing 300 dissolving MNs made from sodium chondroitin sulfate and sampled up to 2 μL of ISF from male Wistar rats within 15 min (Figure 6f). The method was investigated for monitoring vancomycin (VCM—an antibiotic medication) in ISF. A comparison of pharmacokinetic profiles of VCM in ISF and plasma showed similar results and a strong correlation between them.^[100]

4. Biosensors—Sensing and Sampling ISF

Low-cost, minimally invasive, and reliable biosensors that enable real-time and in situ monitoring and detection of clinically relevant biomarkers can dramatically improve patient health care. Continuous biomarker monitoring is crucial, particularly in remote areas, limited-resource settings, and

emergency rooms and intensive care units (ICUs).^[124] Recent pandemics such as COVID-19 have prioritized the need for rapid treatments and the deployment of successful diagnostic strategies to resolve overwhelming pressure on health systems. However, the development and acceptability of POC devices depend on their accuracy, cost-effectiveness, and scalable manufacturing strategies. **Figure 7** shows a general interconnected block diagram of a MN-based biosensor system. MN devices containing working electrodes (WE), counter electrodes (CE), and reference electrodes are connected with the integration unit of the electrical components for off-site or on-site analysis. Power electronics units can be designed to convert signals, analyze data, and interact with other devices, such as mobile phones or laptops, providing more effective disease management in real-time.

Biosensors generally consist of three main parts: 1) a sensing unit to detect the biomarker, 2) a transducer to convert the biosensing event into a measurable signal, and 3) a signal processing unit/power electronics to analyze the signal generated via the transducer (Figure 7).^[125] The combination of these units transfers the biological response to an electrical output that can be measured for further quantitative analysis.^[126]

MNs designed explicitly for direct ISF sampling can also be categorized as on or off-device sensing (Figure 7). On-device detection often requires additional processing steps to analyze the ISF collected by MNs. The technology is still in the experimental stage; however, MN-based biosensors show promising potential for on-device ISF sampling and analysis. Depending on the receptor, a signal produced by the transducer can be either voltage or current (which can be transferred into voltage equivalent). The output voltage is very low and needs amplification to reduce the noise.^[120]

MN-integrated biosensors usually need no external devices or support to conduct the biomolecule analysis, as the aim is to integrate the sensing component into the device. The MN-biosensors mechanism can be simplified into two stages: 1) MNs to extract the biomarker and 2) integrated sensing technology to analyze the sample. Generally, detection techniques for biosensors fall under four categories; calorimetric, electrical, optical, and mechanical. The calorimetric biosensor detects the heat output (or absorbed) of the solution that contains the analyte.^[127] Under electrical detection, spectroscopy, potentiometry, and amperometry are the most common methods.^[128] Techniques such as fluorescence detection, surface plasmon resonance (SPR), surface-enhanced Raman spectroscopy (SERS), colorimetric and photometric detection are mainly used in optical detection.^[129] Mechanical detection includes scanning probe microscopy (SPM), atomic force microscopy (AFM), scanning tunneling microscope (STM), and quartz crystal microbalance (QCM).^[130–133] MN-based biosensors have primarily been researched based on electrochemical detections. Electrochemical biosensors transform the biochemical events (e.g., antigen-antibody reaction) of the sample to an electrical signal where the electrode works as the main component for the immobilization of the biomolecules and movement of the electrons.^[134] Unlike many other techniques, electrochemical biosensors do not require high sensor setup complexity due to their low cost and simple interface. Moreover, electrochemical sensors can also be integrated with wearables for continuous

Microneedle Integrated Biosensor System to Extract ISF and Detect Biomarker

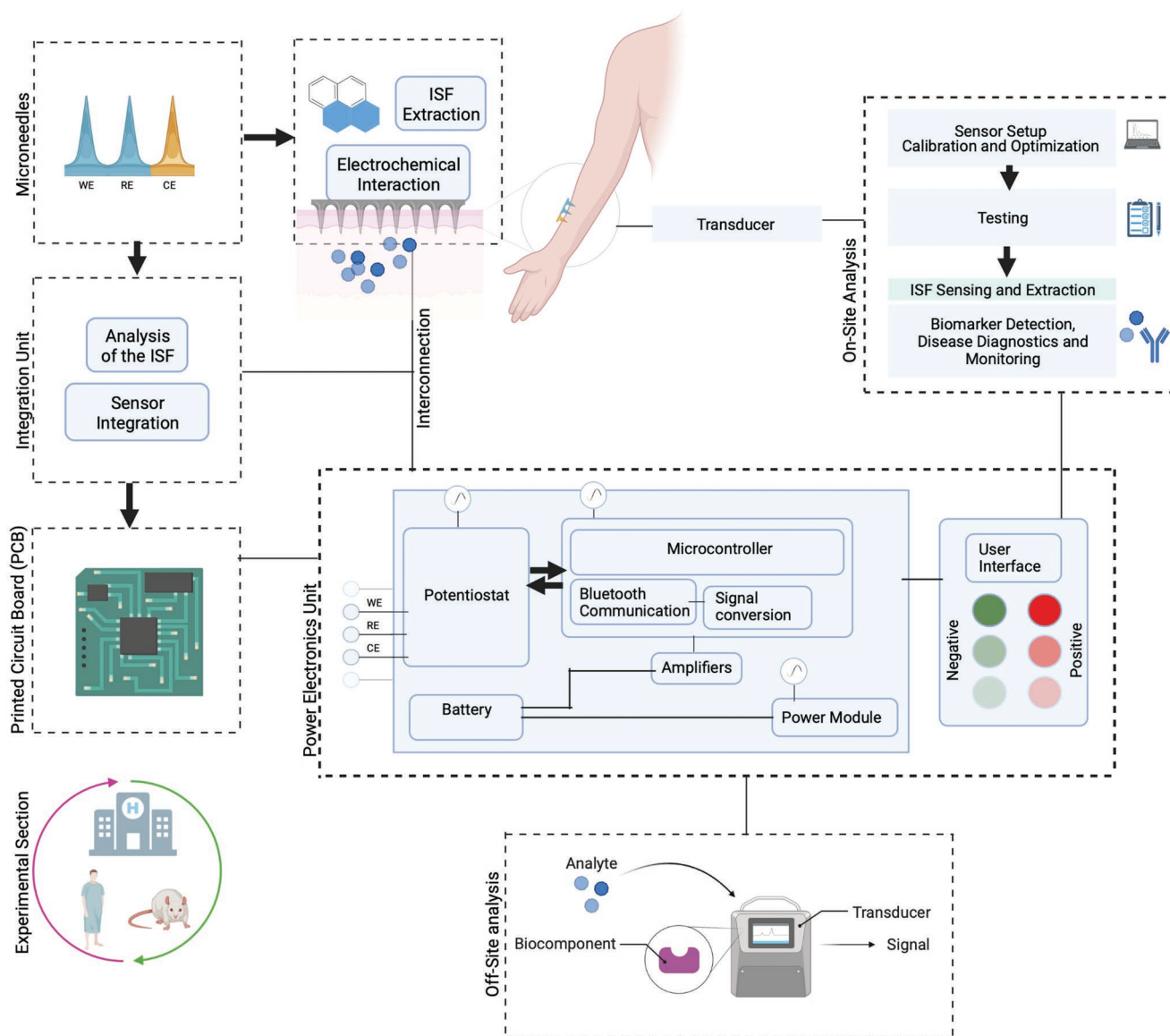


Figure 7. A schematic diagram of a typical MN-based biosensor system consists of a bioreceptor, MNs, an integration unit, a printed circuit board (PCB), a user interface, transducers, and an electronic system (e.g., power electronics). The schematic was created with BioRender.com.

sensing of metabolites in ISF.^[135] Their robustness, miniature size, low power usage, and ability to offer direct and real-time detection of various biomarkers reduce the need for large analytical instruments (e.g., AFM, STM) typically available in laboratories or clinical settings.^[136,137]

4.1. Integrated Hollow MNs

Hollow MN uses common electrodes such as gold, carbon, and platinum to modify the bore for sensing, which measures the difference in electrical potential triggered by an interface

between the analyte present in the tissue fluid and the sensor surface.^[138–140] Various research has focused on glucose detection in ISF using MN-based biosensing technology.^[141,142] Zhao et al. demonstrated the feasibility of a hollow MN-based electrochemical biosensor for glucose detection in ISF with high stability and long-term monitoring. The device was made of three pyramidal MNs (silk/D-sorbitol) combined with silver and platinum wires and immobilized glucose selective enzyme to provide a biocompatible environment for continuous glucose monitoring.^[141] Another study developed a hollow MN with an enzyme-based colorimetric sensor embedded in the channel of the silicon MN for glucose monitoring. The device

extracted ISF by capillary action only, and the result indicated the potential ability of the device to perform continuous glucose monitoring in diabetic patients.^[143] Venugopal et al. developed a wearable sensor to measure the concentration of alcohol in human ISF.^[144] In a recent study, platinum and silver wires were fitted into a hollow MN sensing device and functionalized with an alcohol oxidase enzyme and a reagent layer to continuously monitor alcohol in ISF.^[139] Researchers also demonstrated MN sensing devices for potassium measurement by integrating ion-selective electrodes made of porous carbons or graphene materials with hollow MNs.^[145] Mishra et al. also reported a wearable MN sensor array for the continuous electrochemical detection of fentanyl. The MNs were designed to differentiate between opioid overdose and nerve agent poisoning. The patch was developed with four hollow MNs to detect fentanyl down to the nanomolar level in a skin-mimicking phantom gel.^[137]

Experiments with dual-mode MN-based sensing systems relying on parallel real-time enzymatic-amperometry and non-enzymatic voltammetric techniques using different MNs for the same sensor patch have also been conducted. Goud et al. reported a MN-based sensing platform for continuous monitoring of levodopa (L-Dopa), a medication for treating Parkinson's disease. The sensing experiment was conducted using a MN patch consisting of three hollow MNs where two MNs were prepared from carbon paste, and the third electrode was modified with silver (Ag). The MN sensor patch was tested *ex vivo* by penetrating through mice skin placed on top of an artificial ISF solution containing L-Dopa. As illustrated in Figure 7a-i, direct anodic detection of L-Dopa was achieved using square-wave voltammetry (SWV) for MN (WE1), while the other MN electrode (WE2) used chronoamperometric measurement for the corresponding dopaquinone element. The combination of these two independent detection processes integrated into a single MN platform offers considerable promise toward L-Dopa monitoring and sensing of ISF.^[136] However, the biofouling effect due to the accumulation of protein constituents and other biological materials of the ISF has implications for the performance of the biosensors.^[146,147] To resolve the issue, MNs were coated with a protective Nafion film providing an anti-interference barrier. This rapid detection offered effective analysis and monitoring of L-Dopa in ISF with high sensitivity.^[136]

Silicon is a well-established material for biosensors to construct semiconductor circuits.^[83,142,148] It also has good biocompatibility and has been used for the fabrication of MNs.^[149] Hollow silicon MNs enable passive extraction of ISF using capillary action.^[83] Smith et al. developed a MN array made of silicon with integrated microfluidic channels to extract ISF for analysis of nucleic acid biomarkers. The array contained 400 MNs, of which 200 had bore holes for ISF extraction with a needle-to-needle spacing of 300 μm . The integrated microfluidic channels and reservoir could accommodate 2–3 μL of ISF. The system was designed to be integrated with a sensor for off-chip profiling of nucleic acid constituents. The result demonstrated the identification of potential disease biomarkers which is only achievable using the traditional blood sampling method.^[148]

Dual design concepts such as hollow MNs with solid MNs have been experimented with to improve effective skin penetration.^[92] However, low sampling rates and blockage can occur

during skin penetration.^[88,150] To resolve this issue, various designs have been experimented with, such as varying geometrical structures,^[138] changing the tip angle,^[151] and changing lumen positioning.^[92]

4.2. Integrated Solid MNs

Solid MNs are comparatively economical and easier to fabricate for the development of on-needle electrochemical biosensors. Solid MNs can be coated with gold and platinum nanoparticles to improve conductivity for enzymatic (biological reactions) and non-enzymatic (biological/chemical reaction) analyte detection, eliminating the need for embedding a lumen such as in the case of hollow MNs, which must be filled with pastes or wires. It is reported that solid MN-based electrodes provide improved sensitivity and robustness due to their larger electroactive surface area.^[152,153] Integrated solid MN-based biosensors have been fabricated using silicon or metal and can be coated using techniques such as sputtering and e-beam evaporation to form the electrode with oxidase enzymes for specific biomarker detection.^[152,154–155]

In a study, Sharma et al. developed a continuous glucose monitoring (CGM) system using a solid MN-based biosensor. The device consisted of four MNs made of polycarbonate. Three were coated with platinum and the fourth with silver as a reference electrode. The modified geometry of the MNs allowed them to penetrate dermal tissue without compromising tissue integrity. The outer layer of the solid MNs was adapted as a glucose sensor to observe the real-time change in glucose in ISF. The experiment was conducted using healthy human volunteers for 6 h to analyze pain and tolerability. The results showed a solid performance for glucose sensing for up to 24 h with minimal discomfort.^[156] Data also indicated a time lag, a critical determinant of sensor accuracy, of up to 15 min in a few cases, which could be further offset by sensor calibration. CGM systems can lack accuracy and optimization, limiting them in the clinical setting. A well-developed signal processing method is required to improve CGM performance in future applications.^[156,157] Ming et al. developed a MN patch to measure lactate in ISF continuously. The experiment was part of a clinical trial, and a solid MN patch was applied to the forearm of healthy adult participants undertaking 30 min of exercise. The designed biosensor was well tolerated by the volunteers and detected lactose concentration in ISF in real-time. The reported time lag was around 5 min, and a different pattern was observed between the current flow via biosensor and lactate for the participants in the resting and exercising stages.^[158] Dissolvable polymer coating has also been used on MN with a nanostructure to improve transdermal biosensing. Liu et al. developed a methodology using dissolvable polymers to protect the nanostructure of the MNs. Metal and resins were used to fabricate the MNs, whereas vinyl pyrrolidone was used for coating as a protective layer on the MN surface. MNs were further integrated with a biosensor and applied to the back of the mice's skin to observe the sensing ability of the hydrogen peroxide (H_2O_2) biomarker. The result showed that the sensitivity of the MN-based biosensor without a coating or protective layer was significantly low.^[159]

Cheng et al. developed a touch-actuated glucose sensor integrated with a solid MN array and a dedicated reverse iontophoresis (RI) unit for sampling ISF. The biosensor was designed on three main mechanisms: a MN array consisting of 29 MNs, an integrated RI unit for ISF extraction, and a glucose-sensing unit. The sensor was initially applied to the skin and compressed manually with a finger. MN array penetrated through the skin, creating aqueous microchannels. Once the compression was released, the MN array interacted with the sensor due to rebound energy.^[59] Healthy skin generally contains a high proportion of negative charge. As a result, when the small current is applied to the skin, it flows between the RI electrodes due to the electrokinetic transport mechanism such as electromigration (movement of ions on the flow of the current) and electroosmosis (movement of the ISF-containing ions).^[160–162] The electroosmosis process drives the glucose molecule in ISF to migrate out of the skin through the microchannels towards the RI unit, where the glucose is identified and analyzed. Most of the time, the electroosmotic flow is more significant in microchannels and follows a path with low resistance.^[163] A wireless electromechanical system was also developed based on low-power consumption electronics to deliver the measured data to a smartphone app to share and further process the information. An in vivo experiment was conducted with three healthy diabetic rat groups. Measurement results showed a correlation between the different groups indicating the effectiveness of the biosensor in detecting glucose.^[59] Senel et al. presented an easy method to fabricate a MN array using conductive gold ink to detect urea in artificial ISF. Initially, the MN molds were cleaned, and commercially available gold ink consisting of gold (Au) and polymers was placed in the mold. The mix was centrifuged for two minutes to ensure the efficient penetration of the inks. The front area of the working electrode was coated with insulator ink to reduce signal interference. The biosensing part for urea detection was developed using the urease enzyme. The performance of the electrodes was tested via chronoamperometry to detect the urea concentration in artificial ISF. The results demonstrated successful recognition of urea with higher sensitivity; however, the sensor lacked optimization, proper validation, and implementation in vivo analysis.^[164] **Figure 8** shows various MN-integrated biosensors and their applications.

Kim et al. developed an enzymatic continuous glucose monitoring system with high accuracy for glucose monitoring using MN electrodes. In this study, a mussel adhesive protein was applied to immobilize glucose oxidase on the surface of a MN electrode. The electronic part was designed using a microcontroller unit, signal converter, Bluetooth, and lithium-ion battery. Carbon and Ag/AgCl were printed to produce the electrodes. For accurate performance, the experiment was conducted in vivo at different temperatures. The device was capable of detecting glucose concentration in ISF for up to three days in humans and five days in beagle dogs and showed good performance in comparison with other commercially available disposable glucose sensors.^[166] For the electrodes, conductivity can be maximized by coating MNs with metals such as Au, or non-metals such as carbon paste, carbon fibers, or carbon nanotubes.^[167–172] Skaria et al. developed a cost-effective MN array with nanocomposite films of polylactic acid (PLA) and

carboxyl-functionalized multi-walled carbon nanotubes for dermal biosensing. The solid MN array was fabricated using the micromolding technique and was mechanically robust to withstand skin insertion. The experiment assessed the electrochemical performance in porcine ear skin *ex vivo*. The result showed that the MN biosensor could monitor electrochemical changes in the skin identified by a signature waveform which was further examined through a burn wound model. Signature waveform was used to understand the ability of the MN array to monitor the microenvironmental changes in the skin ISF by comparing the results of an artificial burn site to a nonburn site.^[167] **Table 3** below represents the summarized properties of the previous studies for MN-based ISF extraction and sensing.

5. Conclusions and Future Outlook

ISF is a rich source of biomarkers, but very limited research on clinical trials involving direct ISF sampling exists. This is largely due to a lack of simpler techniques. Conventional methods such as suction blisters and microdialysis require expert support and can be expensive and time-consuming, whereas MNs have been shown to be well tolerated by the skin and have emerged rapidly in research. However, sampling ISF using a MN-based system is a complex process, and most work is limited by the collection of a small volume of fluid and requires the accurate measurement of biomarkers. Many issues have not been fully studied, and further research is required to unlock the maximum potential of MN-based biosensors. **Figure 9** summarizes the key research gaps identified during this study.

Most MN-based biosensors have been designed to detect single biomarkers, demonstrating the significant potential to determine analytes for disease diagnostics.^[173] Successful detection of multiple biomarkers in ISF without the need for drawing blood would enhance diagnostics precision, and therapeutic responsiveness and develop advanced approaches for early diagnosis of various diseases. The volume of ISF extracted by MNs is comparatively low. A small amount of ISF poses the risk of having fewer or no biomarkers. To our knowledge, there is no standard volume of ISF that can offer the guaranteed presence of biomarkers. This must be addressed to overcome barriers associated with the ISF extraction process. Experiments can be conducted to understand the comparison between different ISF volumes and variations in the presence of biomarkers. This will determine the standard volume of ISF and can be very effective in clinical trials. Integration with biosensors needs further investigation to simplify the ISF extraction process. Moreover, exploring new designs of MNs and optimization of biosensors may significantly improve efficiency and accuracy, however, little research has been conducted in this area. The time lag is another issue with ISF sampling that needs further investigation. For example, changes in glucose concentration in plasma and ISF can suggest a time lag of 4–50 min.^[174–178] This indicates when the glucose level changes, the measurement in the ISF may be higher or lower than the actual blood glucose reading.^[179] This physiological delay between blood and ISF poses a critical challenge in developing a continuous blood glucose monitoring system

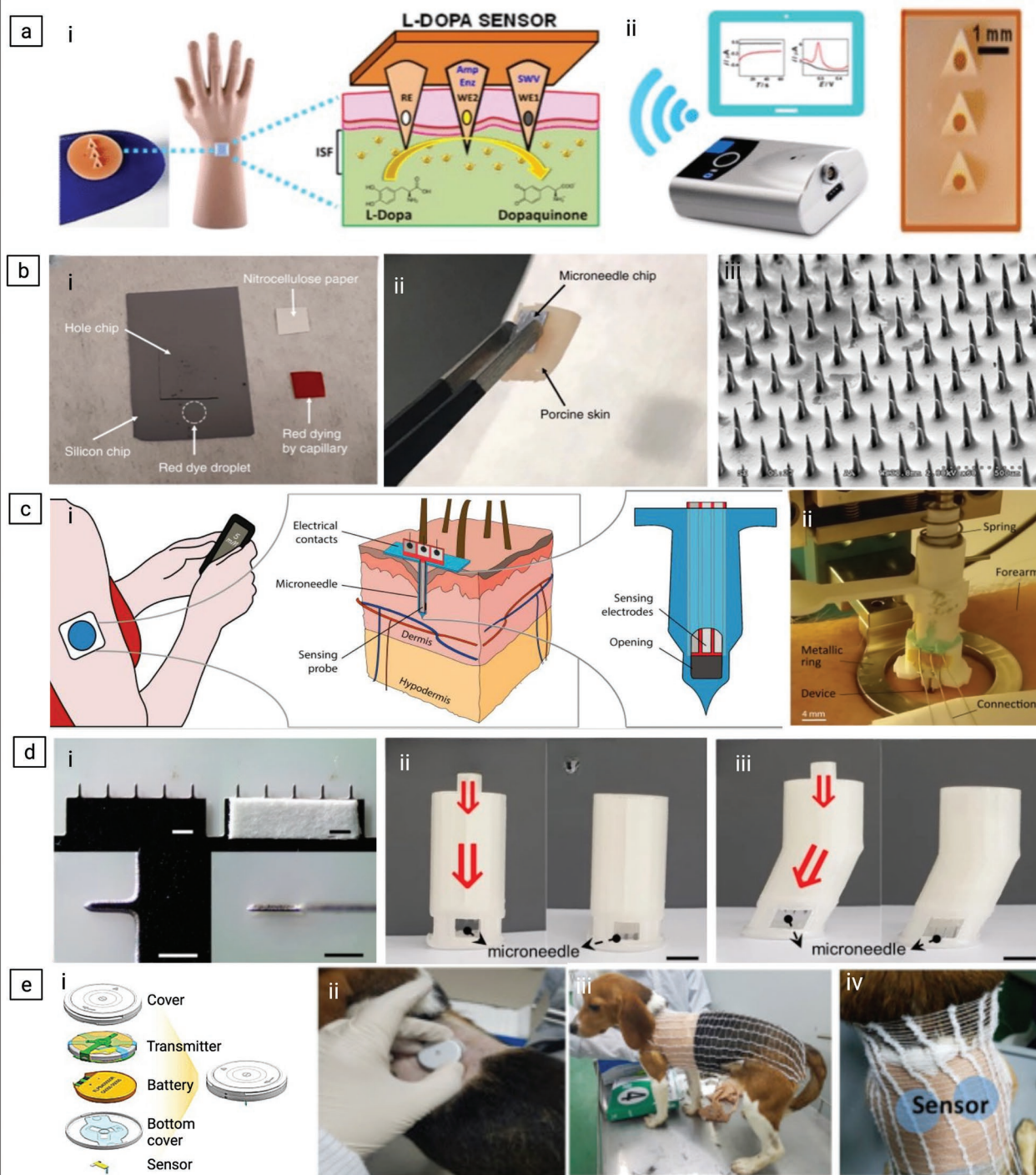


Figure 8. MN-based biosensors for sensing and extracting ISF. a) i) Mannequin hand wearing the MN sensor for L-Dopa detection, ii) wireless communication system for extracted data transmission with an optical image of the MN. Reproduced with permission.^[136] Copyright 2019, American Chemical Society. b) i) Capillary filling of deep-reactive ion etched chip with water solution of red dye, ii) insertion of the MN into the porcine skin, iii) Image of the mechanically intact MNs even after the application. Reproduced under the Creative Commons Attribution License (CC BY 4.0).^[83] Copyright 2019, Springer Nature. c) i) Illustration of the continuous glucose monitoring system with a cross-sectional view of the three sensing electrodes of the MN device. ii) A 3D printed holder integrated into a spring-loaded mechanism with a metal ring to maintain the position of the skin and forearm during the experiment. Reproduced under the Creative Commons Attribution License (CC BY 4.0).^[140] Copyright 2018, Springer. d) i) Optical image of the MNs made of stainless steel, ii) before and after the insertion of the standard MNs. iii) Before and after the insertion of the tilted MNs. Reproduced under the Creative Commons Attribution License (CC BY 4.0).^[165] Copyright 2021, Springer Nature. e) i) Biosensor consists of an integrated transmitter, a lithium-ion battery with the bottom cover integrated with MNs and the sensor, ii) insertion of the sensor on the back of the beagle dog, iii) conducting the in vivo test results. iv) The sensor is attached underneath the wrapped fabric net to hold the position of the device. Reproduced with permission.^[166] Copyright 2019, Elsevier.

Table 3. Summary table of the MN-based biosensor for ISF extraction and sensing that is discussed in this review.

MNs	Materials	Methods	MN length	Object model	Analysis	Year [Ref]
Hollow MNs	Enzyme-modified carbon paste, polymer	Micromachining	700 μm 4 MNs	Skin-mimicking phantom gel	Fentanyl	2020 ^[137]
	Carbon paste, polymer	Square-wave voltammetry chronoamperometry	1500 μm 3 MNs	Mice skin, artificial ISF	Levodopa	2019 ^[136]
	d-sorbitol silk	Molding	800 μm 3 MNs	Artificial ISF	Glucose	2020 ^[141]
	Silicon	Deep-reactive ion etching, wet etching micromachining	$\approx 150 \mu\text{m}$	Porcine skin	–	2019 ^[83]
	Silicon	Deep-reactive ion etching, wet etching	$\approx 400 \mu\text{m}$	Off-chip Profiling	Nucleic acid	2018 ^[148]
	Silicon	Wet etching, deep-reactive ion etching	700 μm 3 MNs	Human forearm	Glucose	2018 ^[140]
	Polymer	3D printing	$\approx 820 \mu\text{m}$ 3 MNs	Porcine skin 2–4 $\mu\text{L Min}^{-1}$	–	2021 ^[165]
	Silicon	3D printing, deep-reactive ion etching	250 μm three-electrode system	Mice skin	Glucose	2022 ^[142]
Solid MNs	Polymers	Laser cutting	1500 μm	Humans, beagle dogs	ISF Glucose	2019 ^[166]
	Carboxyl-multiwalled carbon nanotube	Micromolding	870 μm	Porcine skin	ISF	2019 ^[167]
	Stainless steel resin	Laser etching	600 μm	Anesthetized mice	ISF Hydrogen peroxide	2019 ^[159]
	Polycarbonate	–	–	Humans	Glucose ISF Up to 24 H)	2018 ^[156]
	Stainless steel	Amperometry, reverse iontophoresis	2200 μm 29 MNs	Rabbit skin, rat	Glucose detection	2022 ^[59]
	Gold	Micromolding, chronoamperometry	290 μm 3 \times 3 MNs	–	Artificial ISF	2019 ^[164]
	Polycarbonate	–	$\approx 1000 \mu\text{m}$ 16 MNs	Human forearm	Lactate	2022 ^[158]

with greater accuracy. Reducing the delay (<10 min) might significantly improve system accuracy and effectiveness. The time lag between blood and ISF for different biomarkers also may vary depending on different scenarios (movements or steady conditions). It is suggested that controlled pressure can be applied at the site to increase the blood flow, thus reducing the overall time lag.^[179]

To tailor the results of ISF sampling and disease diagnostics, artificial intelligence (AI) is one of the fields that should be explored. AI will significantly enhance the information collection system, data processing, response time, and decision-making for repetitive tasks. Flexible bioelectronic materials such as polyimide (PI) have been used widely for biosensor integration and can, therefore, be a great support for electrical circuit design facilitating the use of AI MN-based biosensors.^[180] Furthermore, the use of AI has the potential to streamline the process, assist research, provide accurate real-time data, and reduce the need for human interventions. For example, people with cardiovascular diseases require an early and quick diagnosis. The traditional approach to carrying out laboratory results is mostly less effective and time-consuming. Once ISF has been collected by a MN-integrated biosensor, AI can immediately initiate communication with medical professionals,

making the overall system far more sophisticated and effective in critical medical conditions.

Effective analysis of relevant biomarkers is vital for diagnosing and monitoring health conditions, as extraction methods can be time-consuming with relatively low ISF volume. The investigation of appropriate techniques can overcome limitations and accelerate sampling time and detection efficiency. One of the strategies could be the simultaneous monitoring of multiple analytes of ISF at considerably fewer pre- or post-treatment steps. Expanding the range of materials to manufacture MNs would be an ideal option to facilitate prototyping techniques for ISF extraction purposes. For instance, 3D printing technology could simplify the manufacturing process to obtain the desired structure for an ultra-rapid manufacturing process.^[181–183] Continuous discovery of new biomarkers in ISF must also be validated to design clinically successful ISF sampling techniques and MN-based biosensors. High selectivity and sensitivity could be achieved with precise integration between the MN and biosensor. With such functionality, a variety of biomarkers would be easily monitored in the process of acquiring ISF for clinically valuable information.

For optimal application, biosensors need to be programmed for low power consumption using power-efficient electronic

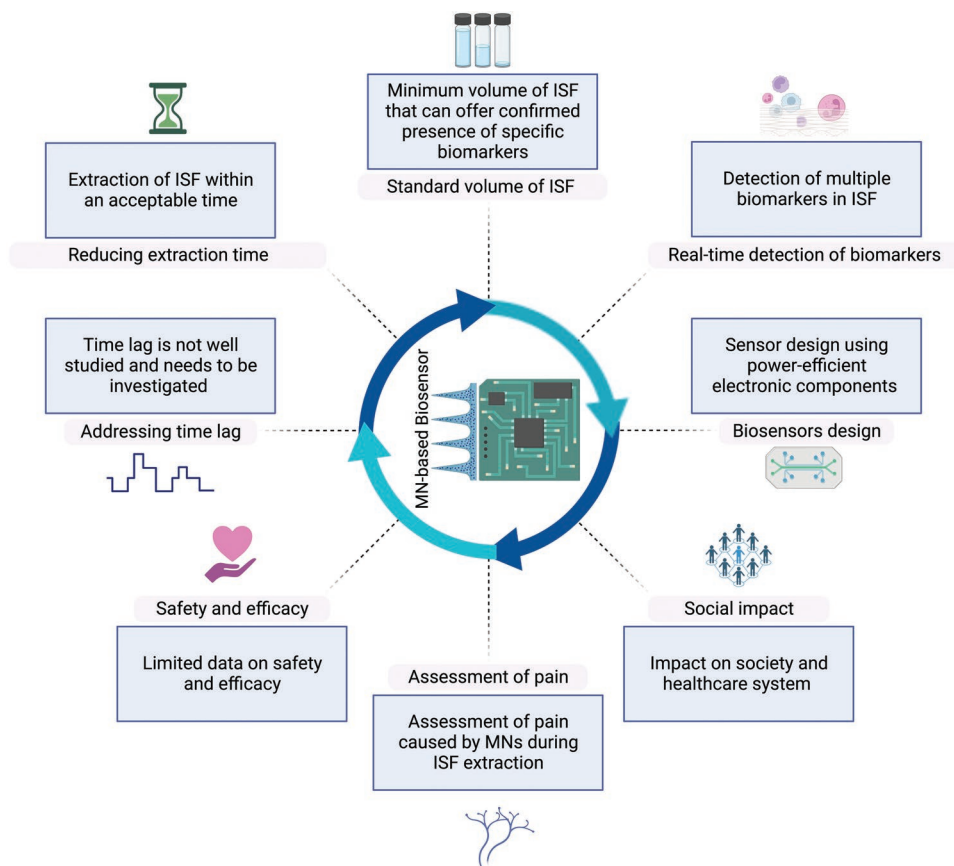


Figure 9. Research gaps identified for successful extraction of ISF using MNs and MN-based biosensors. The schematic was created with BioRender.com.

components and circuit design. However, many biosensors are immature, and the complexity of sampling ISF remains a key challenge. An advanced sampling of ISF would enable the MN-based biosensor to acquire valuable, time-sensitive biomarker information that can be useful for long-term disease diagnosis. Besides continuous glucose monitoring, extensive analysis of other biomarkers requires versatile techniques to extract ISF that may suggest new strategies for at-home POC systems. Such information would significantly improve global healthcare for medical applications regardless of geographical location. A quick and simple sampling method to extract ISF from the skin has the potential for extensive future research in biomarker discovery and monitoring.

Conflict of Interest

The authors declare no conflict of interest.

Keywords

biosensing, biosensors, interstitial fluid, microneedles, point-of-care diagnostics

Received: August 9, 2022

Revised: November 3, 2022

Published online: February 19, 2023

- [1] C. M. McMurtry, R. P. Riddell, A. Taddio, N. Racine, G. J. G. Asmundson, M. Noel, C. T. Chambers, V. Shah, *Clin. J. Pain.* **2015**, *31*, S3.
- [2] J. Biswas, A. Dhali, S. Panja, K. Karpaha, S. Nath, G. K. Dhali, *Cureus* **2022**, *14*, e27458.
- [3] R. Etzioni, N. Urban, S. Ramsey, M. McIntosh, S. Schwartz, B. Reid, J. Radich, G. Anderson, L. Hartwell, *Nat. Rev. Cancer* **2003**, *3*, 243.
- [4] D. B. Matchar, S. R. Love, A. K. Jacobson, R. Edson, L. Uyeda, C. S. Phibbs, R. J. Dolor, *J. Thromb. Thrombolysis* **2015**, *40*, 17.
- [5] S. Sriram, *J. Family Med. Prim. Care* **2019**, *8*, 599.
- [6] J. Kool, L. Reubsat, F. Wesseldijk, R. T. Maravilha, M. W. Pinkse, C. S. D'Santos, J. J. Van Hilten, F. J. Zijlstra, A. J. R. Heck, *Proteomics* **2007**, *7*, 3638.
- [7] J. Heikenfeld, A. Jajack, B. Feldman, S. W. Granger, S. Gaitonde, G. Begtrup, B. A. Katchman, *Nat. Biotechnol.* **2019**, *37*, 407.
- [8] N. J. Abbott, *Neurochem. Int.* **2004**, *45*, 545.
- [9] A. C. Müller, F. P. Breitwieser, H. Fischer, C. Schuster, O. Brandt, J. Colinge, G. Superti-Furga, G. Stingl, A. Elbe-Bürger, K. L. Bennett, *J. Proteome Res.* **2012**, *11*, 3715.
- [10] B. Q. Tran, P. R. Miller, R. M. Taylor, G. Boyd, P. M. Mach, C. N. Rosenzweig, J. T. Baca, R. Polsky, T. Glaros, *J. Proteome Res.* **2018**, *17*, 479.
- [11] M. J. Herfst, H. van Rees, *Arch. Dermatol. Res.* **1978**, *263*, 325.
- [12] S. Kayashima, T. Arai, M. Kikuchi, N. Nagata, N. Ito, T. Kuriyama, J. Kimura, *Am. J. Physiol.* **1992**, *263*, H1623.
- [13] U. Kiistala, *J. Invest. Dermatol.* **1968**, *50*, 129.
- [14] H. S. Gill, D. D. Denson, B. A. Burris, M. R. Prausnitz, *Clin J Pain.* **2008**, *24*, 585.

- [15] J. Gupta, S. Park, B. Bondy, E. I. Felner, M. R. Prausnitz, *Biomaterials*. **2011**, *32*, 6823.
- [16] G. Lee, Y. Ma, Y. ho Lee, H. Jung, *BioChip J.* **2018**, *12*, 309.
- [17] Digital Science. (2018-) Dimensions [Software]. <https://app.dimensions.ai>. (accessed June 2022).
- [18] Y. Luo, Y. Xin, R. Joshi, L. Celi, P. Szolovits, *Proc. Conf. AAAI Artif. Intell.* **2016**, *30*, 42.
- [19] S. F. Berlanda, M. Breitfeld, C. L. Dietsche, P. S. Dittrich, *Anal. Chem.* **2021**, *93*, 311.
- [20] L. Alexandre, A. Bendali, I. Pereiro, M. Azimani, S. Dumas, L. Malaquin, T. D. Mai, S. Descroix, *Sci. Rep.* **2022**, *12*, 9468.
- [21] W. Liu, D. Chen, W. Du, K. P. Nichols, R. F. Ismagilov, *Anal. Chem.* **2010**, *82*, 3276.
- [22] S. Mitragotri, M. Coleman, J. Kost, R. Langer, *J. Appl. Physiol.* **2000**, *89*, 961.
- [23] R. Zhao, C. Wang, F. Lu, L. Du, Z. Fang, X. Guo, J. T. Liu, C. J. Chen, Z. Zhao, *Sensors* **2018**, *18*, 1431.
- [24] H. Wosicka, K. Cal, *J. Dermatol. Sci.* **2010**, *57*, 83.
- [25] U. Blume-Peytavi, A. Vogt, *Br. J. Dermatol.* **2011**, *165*, 13.
- [26] F. Knorr, J. Lademann, A. Patzelt, W. Sterry, U. Blume-Peytavi, A. Vogt, *Eur. J. Pharm. Biopharm.* **2009**, *71*, 173.
- [27] S. Ikeda, K. Naito, R. Imai, M. Manabe, K. Takamori, H. Ogawa, *Br. J. Dermatol.* **1985**, *113*, 661.
- [28] U. Kiistala, K. K. Mustakallio, *Lancet* **1964**, *283*, 1444.
- [29] U. Kiistala, *J. Invest. Dermatol.* **1968**, *50*, 129.
- [30] D. D. Cunningham, J. A. Stenken, in *In Vivo Glucose Sensing*, John Wiley & Sons, **2009**, p. 1.
- [31] L. Heinemann, *Diabetes Technol. Ther.* **2003**, *5*, 545.
- [32] S. Dharadhar, A. Majumdar, S. Dhoble, V. Patravale, *Drug Dev Ind Pharm.* **2019**, *45*, 188.
- [33] Z. Faraji Rad, P. D. Prewett, G. J. Davies, *Beilstein J. Nanotechnol.* **2021**, *12*, 1034.
- [34] V. Ebrahiminejad, P. D. Prewett, G. J. Davies, Z. Faraji Rad, *Adv. Mater. Interfaces* **2022**, *9*, 2101856.
- [35] M. Yuste-Chaves, P. Unamuno-Pérez, *Actas Dermosifiliogr.* **2013**, *104*, 285.
- [36] H. Yousef, M. Alhajj, S. Sharma, *Anatomy, Skin (Integument), Epidermis*, StatPearls Publishing, FL **2022**, <https://www.ncbi.nlm.nih.gov/books/NBK470464/>.
- [37] S. Nafisi, H. I. Maibach, *Emerging Nanotechnologies in Immunology*, Elsevier, Amsterdam **2018**, pp. 47–88.
- [38] E. Kahraman, S. Güngör, Y. Özsoy, *Ther. Delivery* **2017**, *8*, 967.
- [39] B. Godin, E. Touthou, *Encycl. Nanotechnol.* **2012**, https://link.springer.com/referenceworkentry/10.1007/978-90-481-9751-4_81.
- [40] J. Zhang, C. H. Purdon, E. W. Smith, *Am. J. Drug Delivery* **2006**, *4*, 215.
- [41] H.-H. Hsu, K. Schimek, U. Marx, R. Pörtner, *Measurement and Simulation of Permeation and Diffusion in Native and Cultivated Tissue Constructs*, Biomaterials in Regenerative Medicine, London, United Kingdom **2018**, <https://doi.org/10.5772/intechopen.72904>.
- [42] C. M. Lopes, J. Silva, M. E. C. D. Real Oliveira, M. Lúcio, *Design of Nanostructures for Versatile Therapeutic Applications*, William Andrew, Norwich, NY, **2018**, pp. 565–622.
- [43] R. K. Keservani, S. Bandopadhyay, N. Bandyopadhyay, A. K. Sharma, *Drug Delivery Syst.* **2019**, <https://doi.org/10.1016/B978-0-12-814487-9.00004-1>.
- [44] C. L. Fang, I. A. Aljuffali, Y. C. Li, J. Y. Fang, *Ther. Delivery* **2014**, *5*, 991.
- [45] A. P. Raphael, G. Garrastazu, F. Sonvico, T. W. Prow, *Ther. Delivery* **2015**, *6*, 197.
- [46] H. Wiig, M. A. Swartz, *Physiol. Rev.* **2012**, *92*, 1005.
- [47] T. A. Hakala, A. García Pérez, M. Wardale, I. A. Ruuth, R. T. Vänskä, T. A. Nurminen, E. Kemp, Z. A. Boeva, J.-M. Alakoskela, K. Pettersson-Fernholm, E. Hæggröm, J. Bobacka, *Sci. Rep.* **2021**, *11*, 7609.
- [48] P. P. Samant, M. R. Prausnitz, in 19th Int. Conf. on Miniaturized Systems for Chemistry and Life Sciences, Chemical and Biological Microsystems Society (CBMS), Gyeongju, **2015**.
- [49] C. Wang, Z. Ma, T. Wang, Z. Su, *Adv. Funct. Mater.* **2006**, *16*, 1673.
- [50] E. Bajramaj, B. Häggman-Henrikson, A. Dawson, B. Gerdle, B. Ghafouri, *Diagnostics* **2019**, *9*, 14.
- [51] A. Alexander, S. Dwivedi, Ajazuddin, T. K. Giri, S. Saraf, S. Saraf, D. K. Tripathi, *J. Controlled Release* **2012**, *164*, 26.
- [52] G. Merino, Y. N. Kalia, M. B. Delgado-Charro, R. O. Potts, R. H. Guy, *J. Controlled Release* **2003**, *88*, 85.
- [53] A. Nair, S. Prakash, A. Goel, A. Kumar, *J. Basic Clin. Pharm.* **2012**, *3*, 207.
- [54] E. Vranić, *Bosn. J. Basic Med. Sci.* **2003**, *3*, 54.
- [55] O. Seror, *Diagn. Interv. Imaging* **2015**, *96*, 617.
- [56] S. Gebhart, M. Faupel, R. Fowler, C. Kapsner, D. Lincoln, V. McGee, J. Pasqua, L. Steed, M. Wangsness, F. Xu, M. Vanstoy, *Glucose Sensing in Transdermal Body Fluid Collected Under Continuous Vacuum Pressure Via Micropores in the Stratum Corneum*, Diabetes Technology & Therapeutics, **2003**, pp. 159–166, <http://doi.org/10.1089/152091503321827812>.
- [57] C. Kolluru, M. Williams, J. Chae, M. R. Prausnitz, *Adv. Healthcare Mater.* **2019**, *8*, 1801262.
- [58] P. P. Samant, M. R. Prausnitz, *Proc. Natl. Acad. Sci. U. S. A.* **2018**, *115*, 4583.
- [59] Y. Cheng, X. Gong, J. Yang, G. Zheng, Y. Zheng, Y. Li, Y. Xu, G. Nie, X. Xie, M. Chen, C. Yi, L. Jiang, *Biosens. Bioelectron.* **2022**, *203*, 114026.
- [60] Z. Pu, C. Zou, R. Wang, X. Lai, H. Yu, K. Xu, D. Li, *Biomicrofluidics* **2016**, *10*, 011910.
- [61] D. Li, R. Wang, H. Yu, G. Li, Y. Sun, W. Liang, K. Xu, *Sensors* **2014**, *14*, 7084.
- [62] X. Xu, H. Zhang, Y. Yan, J. Wang, L. Guo, *Acta Mech. Sin.* **2021**, *37*, 1843.
- [63] S. Chakrabarty, J. Bhattacharya, A. Chowdhury, P. Roy, S. K. Jha, *Int. J. Appl. Pharm.* **2022**, *14*, 26.
- [64] R. O. Potts, J. A. Tamada, M. J. Tierney, *Diabetes Metab. Res. Rev.* **2002**, *18*, S49.
- [65] A. Sieg, R. H. Guy, M. B. Delgado-Charro, *Clin. Chem.* **2004**, *50*, 1383.
- [66] U. Sjöbom, K. Christenson, A. Hellström, A. K. Nilsson, *Front. Immunol.* **2020**, *11*, 2869.
- [67] M. M. Niedzwiecki, P. Samant, D. I. Walker, V. Tran, D. P. Jones, M. R. Prausnitz, G. W. Miller, *Anal. Chem.* **2018**, *90*, 3786.
- [68] L. L. Holm, M. Vukmanovic-Stejic, T. Blauenfeldt, T. Benfield, P. Andersen, A. N. Akbar, M. Ruhwald, *J. Vis. Exp.* **2018**, *11*, 57554.
- [69] A. L. Krogstad, P. A. Jansson, P. Gisslén, P. Lönnroth, *Br. J. Dermatol.* **1996**, *134*, 1005.
- [70] O. Lönnroth, P. A. Jansson, U. Smith, *Am. J. Physiol.* **1987**, *253*, E228.
- [71] S. Schmidt, R. Banks, V. Kumar, K. H. Rand, H. Derendorf, *J. Clin. Pharmacol.* **2008**, *48*, 351.
- [72] H. S. Gill, M. R. Prausnitz, *J. Diabetes Sci. Technol.* **2007**, *1*, 725.
- [73] J. Lenicek Krljeza, A. Dorotic, A. Grzunov, M. Maradin, *Biochem. Med. (Zagreb)* **2015**, *25*, 335.
- [74] S. Stancliff, B. Agins, J. D. Rich, S. Burris, *BMC Public Health* **2003**, *3*, 37.
- [75] R. F. Donnelly, T. R. R. Singh, M. M. Tunney, D. I. J. Morrow, P. A. McCarron, C. O'Mahony, A. D. Woolfson, *Pharm. Res.* **2009**, *26*, 2513.

- [76] T. R. R. Singh, H. Mcmillan, K. Mooney, A. Z. Alkilani, R. F. Donnelly, *Microneedles for Drug Delivery and Monitoring*, Elsevier Inc., **2013**, pp. 185–230, <https://doi.org/10.1533/9780857097040.2.185>.
- [77] M. G. McGrath, A. Vrdoljak, C. O'Mahony, J. C. Oliveira, A. C. Moore, A. M. Crean, *Int. J. Pharm.* **2011**, *415*, 140.
- [78] R. F. Carvalhal, M. S. Kfoury, M. H. O. de Piazetta, A. L. Gobbi, L. T. Kubota, *Anal. Chem.* **2010**, *82*, 1162.
- [79] A. W. Martinez, S. T. Phillips, Z. Nie, C. M. Cheng, E. Carrilho, B. J. Wiley, G. M. Whitesides, *Lab Chip* **2010**, *10*, 2499.
- [80] H. J. G. E. Gardeniers, R. Lutge, E. J. W. Berenschot, M. J. de Boer, S. Y. Yeshurun, M. Hefetz, R. Van't Oever, A. van den Berg, *J. Microelectromech. Syst.* **2003**, *12*, 855.
- [81] P. P. Samant, M. M. Niedzwiecki, N. Raviele, V. Tran, J. Mena-Lapaix, D. I. Walker, E. I. Felner, D. P. Jones, G. W. Miller, M. R. Prausnitz, *Sci. Transl. Med.* **2020**, *12*, <https://doi.org/10.1126/scitranslmed.aaw0285>.
- [82] P. M. Wang, M. Cornwell, M. R. Prausnitz, *Diabetes Technol. Ther.* **2005**, *7*, 131.
- [83] Y. Li, H. Zhang, R. Yang, Y. Laffitte, U. Schmill, W. Hu, M. Kaddoura, E. J. M. Blondeel, B. Cui, *Microsyst. Nanoeng.* **2019**, *5*, 41.
- [84] K. J. Krieger, N. Bertollo, M. Dangol, J. T. Sheridan, M. M. Lowery, E. D. O'Cearbhaill, *Microsyst. Nanoeng.* **2019**, *5*, 42.
- [85] Z. Faraji Rad, P. D. Prewett, G. J. Davies, *Manuf. Lett.* **2021**, *30*, 39.
- [86] Z. Faraji Rad, R. E. Nordon, C. J. Anthony, L. Bilston, P. D. Prewett, J.-Y. Arns, C. H. Arns, L. Zhang, G. J. Davies, *Microsyst. Nanoeng.* **2017**, *3*, 17034.
- [87] Z. Faraji Rad, P. D. Prewett, G. J. Davies, *Addit. Manuf.* **2022**, *56*, 102953.
- [88] C. G. Li, C. Y. Lee, K. Lee, H. Jung, *Biomed. Microdevices* **2013**, *15*, 17.
- [89] Z. Faraji Rad, *Microneedles Fabrication for Subcutaneous Fluid Sampling and Drug Delivery*, University of Birmingham, College of Engineering and Physical Sciences, Birmingham **2016**.
- [90] Z. Faraji Rad, R. E. Nordon, G. J. Davies, C. J. Anthony, P. Prewett, *US Patent 10850082*, **2020**.
- [91] P. R. Miller, R. M. Taylor, B. Q. Tran, G. Boyd, T. Glaros, V. H. Chavez, R. Krishnakumar, A. Sinha, K. Poorey, K. P. Williams, S. S. Branda, J. T. Baca, R. Polsky, *Commun. Biol.* **2018**, *1*, 173.
- [92] E. V. Mukerjee, S. D. Collins, R. R. Isseroff, R. L. Smith, *Sens. Actuators A Phys.* **2004**, *114*, 267.
- [93] R. M. Taylor, D. Maharjan, F. Moreu, J. T. Baca, *Microsyst. Technol.* **2020**, *26*, 2067.
- [94] J. Gupta, E. I. Felner, M. R. Prausnitz, *Diabetes Technol. Ther.* **2009**, *11*, 329.
- [95] J. J. Norman, M. R. Brown, N. A. Raviele, M. R. Prausnitz, E. I. Felner, *Pediatr. Diabetes* **2013**, *14*, 459.
- [96] J. J. Norman, S. O. Choi, N. T. Tong, A. R. Aiyar, S. R. Patel, M. R. Prausnitz, M. G. Allen, *Biomed. Microdevices* **2013**, *15*, 203.
- [97] P. Zhang, C. Dalton, G. A. Jullien, *Microsyst. Technol.* **2009**, *15*, 1073.
- [98] A. Ranzoni, M. A. Cooper, in *Micro and Nano Technologies*, (Eds.: M. Skwarczynski, I. Toth), William Andrew Publishing **2017**, <https://doi.org/10.1016/B978-0-323-39981-4.00001-4>.
- [99] H. Chang, M. Zheng, X. Yu, A. Than, R. Z. Seeni, R. Kang, J. Tian, D. P. Khanh, L. Liu, P. Chen, C. Xu, *Adv. Mater.* **2017**, *29*, 1702243.
- [100] Y. Ito, Y. Inagaki, S. Kobuchi, K. Takada, T. Sakaeda, *Int. J. Med. Sci.* **2016**, *13*, 271.
- [101] M. Zheng, Z. Wang, H. Chang, L. Wang, S. W. T. Chew, D. C. S. Lio, M. Cui, L. Liu, B. C. K. Tee, C. Xu, *Adv. Healthcare Mater.* **2020**, *9*, 1901683.
- [102] R. He, Y. Niu, Z. Li, A. Li, H. Yang, F. Xu, F. Li, *Adv. Healthcare Mater.* **2020**, *9*, 1901201.
- [103] D. al Sulaiman, J. Y. H. Chang, N. R. Bennett, H. Topouzi, C. A. Higgins, D. J. Irvine, S. Ladame, *ACS Nano* **2019**, *13*, 9620.
- [104] N. Xu, M. Zhang, W. Xu, G. Ling, J. Yu, P. Zhang, *Analyst* **2022**, *147*, 1478.
- [105] Y. Qiao, J. Du, R. Ge, H. Lu, C. Wu, J. Li, S. Yang, S. Zada, H. Dong, X. Zhang, *Anal. Chem.* **2022**, *94*, 5538.
- [106] J. Chen, M. Wang, Y. Ye, Z. Yang, Z. Ruan, N. Jin, *Biomed. Microdevices* **2019**, *21*, 63.
- [107] R. F. Donnelly, T. R. Raj Singh, A. D. Woolfson, *Drug Delivery* **2010**, *17*, 187.
- [108] M. J. Garland, T. R. R. Singh, A. D. Woolfson, R. F. Donnelly, *Int. J. Pharm.* **2011**, *406*, 91.
- [109] M. I. Baker, S. P. Walsh, Z. Schwartz, B. D. Boyan, *J. Biomed. Mater. Res. B Appl. Biomater.* **2012**, *100B*, 1451.
- [110] S. Yang, Y. Feng, L. Zhang, N. Chen, W. Yuan, T. Jin, *Int J Nano-medicine* **2012**, *7*, 1415.
- [111] E. A. Kamoun, X. Chen, M. S. Mohy Eldin, E. R. S. Kenawy, *Arabian J. Chem.* **2015**, *8*, 1.
- [112] Y. Piao, H. You, T. Xu, H.-P. Bei, I. Z. Piwko, Y. Y. Kwan, X. Zhao, *Eng. Regener.* **2021**, *2*, 47.
- [113] Q. Chai, Y. Jiao, X. Yu, *Gels* **2017**, *3*, 6.
- [114] H. Du, P. Liu, J. Zhu, J. Lan, Y. Li, L. Zhang, J. Zhu, J. Tao, *ACS Appl. Mater. Interfaces* **2019**, *11*, 43588.
- [115] L. A. Shah, M. Khan, R. Javed, M. Sayed, M. S. Khan, A. Khan, M. Ullah, *J. Clean Prod.* **2018**, *201*, 78.
- [116] E. Laszlo, G. de Crescenzo, A. Nieto-Argüello, X. Banquy, D. Brambilla, *Adv. Funct. Mater.* **2021**, *31*, 2106061.
- [117] X. Chen, G. J. P. Fernando, M. L. Crichton, C. Flaim, S. R. Yukiko, E. J. Fairmaid, H. J. Corbett, C. A. Primiero, A. B. Ansaldo, I. H. Frazer, L. E. Brown, M. A. F. Kendall, *J. Controlled Release* **2011**, *152*, 349.
- [118] P. Van Damme, F. Oosterhuis-Kafeja, M. Van der Wielen, Y. Almagor, O. Sharon, Y. Levin, *Vaccine* **2009**, *27*, 454.
- [119] M. H. Ling, M. C. Chen, *Acta Biomater.* **2013**, *9*, 8952.
- [120] M. C. Chen, S. F. Huang, K. Y. Lai, M. H. Ling, *Biomaterials* **2013**, *34*, 3077.
- [121] J. W. Lee, S. O. Choi, E. I. Felner, M. R. Prausnitz, *Small* **2011**, *7*, 531.
- [122] A. Malek-Khatabi, Z. Faraji Rad, M. Rad-Malekshahi, H. Akbarijavar, *Mater. Lett.* **2023**, *330*, 133328.
- [123] K. van der Maaden, W. Jiskoot, J. Bouwstra, *J. Controlled Release* **2012**, *161*, 645.
- [124] Y. Luo, Y. Xin, R. Joshi, L. Celi, P. Szolovits, *Proc. Conf. AAAI Artif. Intell.* **2016**, *30*, <https://doi.org/10.1609/aaai.v30i1.9998>.
- [125] S. Cagnin, M. Caraballo, C. Guiducci, P. Martini, M. Ross, M. Santaana, D. Danley, T. West, G. Lanfranchi, *Sensors (Basel)* **2009**, *9*, 3122.
- [126] L. Soleymani, F. Li, *ACS Sens.* **2017**, *2*, 458.
- [127] H. G. Hundedek, M. Weiß, T. Scheper, F. Schubert, *Biosens. Bioelectron.* **1993**, *8*, 205.
- [128] A. A. Karyakin, O. A. Bobrova, L. V. Lukachova, E. E. Karyakina, *Sens. Actuators B Chem.* **1996**, *33*, 34.
- [129] J. Ali, J. Najeel, M. Asim Ali, M. Farhan Aslam, A. Raza, *J. Biosens. Bioelectron.* **2017**, *08*, <https://doi.org/10.4172/2155-6210.1000235>.
- [130] C. K. O'Sullivan, G. G. Guilbault, *Biosens. Bioelectron.* **1999**, *14*, 663.
- [131] W. Ohtani, T. Ohda, A. Sumi, K. Kobayashi, T. Ohmura, *Anal. Chem.* **1998**, *70*, 425.
- [132] S. Husale, H. H. J. Persson, O. Sahin, *Nature* **2009**, *462*, 1075.
- [133] G. Binnig, H. Rohrer, C. Gerber, E. Weibel, *Surf. Sci.* **1983**, *131*, L379.

- [134] H. Zheng, X. Ma, L. Chen, Z. Lin, L. Guo, B. Qiu, G. Chen, *Anal. Methods* **2013**, *5*, 5005.
- [135] F. Tehrani, H. Teymourian, B. Wuerstle, J. Kavner, R. Patel, A. Furmidge, R. Aghavali, H. Hosseini-Toudeshki, C. Brown, F. Zhang, K. Mahato, Z. Li, A. Barfidokht, L. Yin, P. Warren, N. Huang, Z. Patel, P. P. Mercier, J. Wang, *Nat. Biomed. Eng.* **2022**, *6*, 1214.
- [136] K. Y. Goud, C. Moonla, R. K. Mishra, C. Yu, R. Narayan, I. Litvan, J. Wang, *ACS Sens.* **2019**, *4*, 2196.
- [137] R. K. Mishra, K. Y. Goud, Z. Li, C. Moonla, M. A. Mohamed, F. Tehrani, H. Teymourian, J. Wang, *J. Am. Chem. Soc.* **2020**, *142*, 5991.
- [138] A. Jina, M. J. Tierney, J. A. Tamada, S. McGill, S. Desai, B. Chua, A. Chang, M. Christiansen, *J. Diabetes Sci. Technol.* **2014**, *8*, 483.
- [139] A. M. V. Mohan, J. R. Windmiller, R. K. Mishra, J. Wang, *Biosens. Bioelectron.* **2017**, *91*, 574.
- [140] F. Ribet, G. Stemme, N. Roxhed, *Biomed. Microdevices* **2018**, *20*, 101.
- [141] L. Zhao, Z. Wen, F. Jiang, Z. Zheng, S. Lu, *RSC Adv.* **2020**, *10*, 6163.
- [142] M. Dervisevic, M. Alba, L. Yan, M. Senel, T. R. Gengenbach, B. Prieto-Simon, N. H. Voelcker, *Adv. Funct. Mater.* **2022**, *32*, 2009850.
- [143] F. Ribet, G. Stemme, N. Roxhed, *Biomed. Microdevices* **2018**, *20*, 101.
- [144] M. Venugopal, K. E. Feuvrel, D. Mongin, S. Bambot, M. Faupel, A. Panangadan, A. Talukder, R. Pidva, *IEEE Sens. J.* **2008**, *8*, 71.
- [145] P. R. Miller, X. Xiao, I. Brener, D. B. Burckel, R. Narayan, R. Polsky, *Biopolymers* **2013**, *3*, 876.
- [146] B. L. Hanssen, S. Siraj, D. K. Y. Wong, *Rev. Anal. Chem.* **2016**, *35*, 1.
- [147] S. Campuzano, M. Pedrero, P. Yáñez-Sedeño, J. M. Pingarrón, *Int. J. Mol. Sci.* **2019**, *20*, 423.
- [148] R. L. Smith, S. D. Collins, J. Duy, T. D. Minogue, in *Microfluidics, BioMEMS, and Medical Microsystems XVI* (Eds.: B. L. Gray, H. Becker), SPIE, **2018**, p. 1049102.
- [149] D. Saadat-Moghaddam, J. H. Kim, *Sensors* **2017**, *17*, 1883.
- [150] D. S. Lee, C. G. Li, C. Ihm, H. Jung, *Sens. Actuators B Chem.* **2018**, *255*, 384.
- [151] S. Aoyagi, H. Izumi, M. Fukuda, *Sens. Actuators A Phys.* **2008**, *143*, 20.
- [152] A. R. B. Moniz, K. Michelakis, J. Trzebinski, S. Sharma, D. G. Johnston, N. Oliver, A. Cass, *J. Diabetes Sci. Technol.* **2012**, *6*, 479.
- [153] J. Trzebinski, S. Sharma, A. Radomska-Botelho Moniz, K. Michelakis, Y. Zhang, A. E. G. Cass, *Lab Chip* **2011**, *12*, 348.
- [154] D. H. Keum, H. S. Jung, T. Wang, M. H. Shin, Y. E. Kim, K. H. Kim, G. O. Ahn, S. K. Hahn, *Adv. Healthcare Mater.* **2015**, *4*, 1153.
- [155] S. A. Skoog, P. R. Miller, R. D. Boehm, A. v. Sumant, R. Polsky, R. J. Narayan, *Diam. Relat. Mater.* **2015**, *54*, 39.
- [156] S. Sharma, A. El-Laboudi, M. Reddy, N. Jugnee, S. Sivasubramaniyam, M. el Sharkawy, P. Georgiou, D. Johnston, N. Oliver, A. E. G. Cass, *Anal. Methods* **2018**, *10*, 2088.
- [157] A. Facchinetti, *Sensors (Basel)* **2016**, *16*, 2093.
- [158] D. K. Ming, S. Jangam, S. A. N. Gowers, R. Wilson, D. M. E. Freeman, M. G. Boutelle, A. E. G. Cass, D. O'Hare, A. H. Holmes, *BMJ Innov.* **2022**, *8*, 87.
- [159] F. Liu, Z. Lin, Q. Jin, Q. Wu, C. Yang, H.-J. Chen, Z. Cao, D.-A. Lin, L. Zhou, T. Hang, G. He, Y. Xu, W. Xia, J. Tao, X. Xie, *ACS Appl. Mater. Interfaces* **2019**, *11*, 4809.
- [160] T. W. Wong, *J. Controlled Release* **2014**, *193*, 257.
- [161] S.-R. Kwon, S. H. Nam, C. Y. Park, S. Baek, J. Jang, X. Che, S. H. Kwak, Y.-R. Choi, N.-R. Park, J.-Y. Choi, Y. Lee, T. D. Chung, *Adv. Funct. Mater.* **2018**, *28*, 1705952.
- [162] P. Charoenputtakun, S. K. Li, T. Ngawhirunpat, *Int. J. Pharm.* **2015**, *495*, 318.
- [163] E. R. Scott, A. I. Laplaza, H. S. White, J. B. Phipps, *Pharm. Res.* **1993**, *10*, 1699.
- [164] M. Senel, M. Dervisevic, N. H. Voelcker, *Mater. Lett.* **2019**, *243*, 50.
- [165] S. Kim, M. S. Lee, H. S. Yang, J. H. Jung, *Sci. Rep.* **2021**, *11*, 14018.
- [166] K. B. Kim, H. Choi, H. J. Jung, Y. J. Oh, C. H. Cho, J. H. Min, S. Yoon, J. Kim, S. J. Cho, H. J. Cha, *Biosens. Bioelectron.* **2019**, *143*, 111622.
- [167] E. Skaria, B. A. Patel, M. S. Flint, K. W. Ng, *Anal. Chem.* **2019**, *91*, 4436.
- [168] P. R. Miller, S. A. Skoog, T. L. Edwards, D. M. Lopez, D. R. Wheeler, D. C. Arango, X. Xiao, S. M. Brozik, J. Wang, R. Polsky, R. J. Narayan, *Talanta* **2012**, *88*, 739.
- [169] G. Valdés-Ramírez, Y.-C. Li, J. Kim, W. Jia, A. J. Bandodkar, R. Nuñez-Flores, P. R. Miller, S.-Y. Wu, R. Narayan, J. R. Windmiller, R. Polsky, J. Wang, *Electrochem. Commun.* **2014**, *47*, 58.
- [170] P. Bollella, S. Sharma, A. E. G. Cass, R. Antiochia, *Biosens. Bioelectron.* **2019**, *123*, 152.
- [171] C. Barrett, K. Dawson, C. O'Mahony, A. O'Riordan, *ECS J. Solid State Sci. Technol.* **2015**, *4*, S3053.
- [172] K. B. Kim, W. C. Lee, C. H. Cho, D. S. Park, S. J. Cho, Y. B. Shim, *Sens. Actuators B Chem.* **2019**, *281*, 14.
- [173] E. C. Lee, M. S. Fragala, S. A. Kavouras, R. M. Queen, J. L. Pryor, D. J. Casa, *J. Strength Cond. Res.* **2017**, *31*, 2920.
- [174] M. S. Boyne, D. M. Silver, J. Kaplan, C. D. Saudek, *Diabetes* **2003**, *52*, 2790.
- [175] K. J. Wientjes, P. Vonk, Y. Vonk-Van Klei, A. J. M. Schoonen, N. W. Kossen, *Diabetes Care* **1998**, *21*, 1481.
- [176] K. Jungheim, K. J. Wientjes, L. Heinemann, V. Lodwig, T. Koschinsky, A. J. Schoonen, *Diabetes Care* **2001**, *24*, 1696.
- [177] L. M. Hullegie, H. L. Lutgers, R. P. F. Dullaart, W. J. Sluiter, K. J. Wientjes, A. J. M. Schoonen, K. Hoogenberg, *Neth. J. Med.* **2000**, *57*, 13.
- [178] H. L. Lutgers, L. M. Hullegie, K. Hoogenberg, W. J. Sluiter, R. P. F. Dullaart, K. J. Wientjes, A. J. M. Schoonen, *Neth. J. Med.* **2000**, *57*, 7.
- [179] P. J. Stout, J. R. Racchini, M. E. Hilgers, *Diabetes Technol. Ther.* **2004**, *6*, 635.
- [180] X. Jin, C. Liu, T. Xu, L. Su, X. Zhang, *Biosens. Bioelectron.* **2020**, *165*, 112412.
- [181] Z. Faraji Rad, P. D. Prewett, G. J. Davies, *Microsyst. Nanoeng.* **2021**, *7*, 71.
- [182] V. Ebrahiminejad, Z. Faraji Rad, *Adv. Mater. Interfaces* **2022**, *9*, 2201115.
- [183] V. Ebrahiminejad, Z. Faraji Rad, P. D. Prewett, G. J. Davies, *Beilstein J. Nanotechnol.* **2022**, *13*, 629.



Khaled Mohammed Saifullah completed his B.Sc. in electrical and electronics engineering at the American International University—Bangladesh (2015) and obtained his M.Sc. in electrical engineering from the University of New South Wales (2019). He is currently a Ph.D. candidate at the University of Southern Queensland under the supervision of Dr. Zahra Faraji Rad. His current research interest focuses on designing and developing microneedle-based biosensors for point-of-care diagnostics, including biomarker detection, ISF extraction, and microelectrodes.



Zahra Faraji Rad is a senior lecturer in mechanical engineering at the University of Southern Queensland. She received a M.Eng. with 1st Class Honors in biomedical engineering from the University of Birmingham (2010). She obtained her Ph.D. from the Universities of New South Wales and Birmingham as the first joint Ph.D. candidate from the two universities under the international Universitas 21 partnership (2016). Her current research interests include microneedles for point-of-care diagnostics and drug delivery. She is the recipient of 2021 Science and Innovation Awards for Young People in Agriculture, Fisheries and Forestry in the CSIRO Biosecurity digital innovation Award category.